Spring 5-15-2019

Activation of Toll-like Receptor 3 Translates to Long-term Post-viral Lung Disease

Xinyu Wang
Washington University in St. Louis

WASHINGTON UNIVERSITY IN ST. LOUIS

Division of Biology & Biomedical Sciences
Immunology

Dissertation Examination Committee:
Michael Holtzman, Chair
Gaya Amarasinghe
John Atkinson
Mark Miller
Rodney Newberry
Wayne Yokoyama

Activation of Toll-like Receptor 3 Translates to Long-term Post-viral Lung Disease

by
Xinyu Wang

A dissertation presented to
The Graduate School
of Washington University in
partial fulfillment of the
requirements for the degree
of Doctor of Philosophy

May 2019
St. Louis, Missouri

Table of Contents

List of Figures

List of Abbreviations

BMDC	Bone marrow-derived dendritic cell
CCR2	C-C motif chemokine receptor 2
cDC	Conventional dendritic cell
dpi	Days post-infection
COPD	Chronic obstructive pulmonary disease
DC	Dendritic cell
FEV_1	Forced expiratory volume in one second
IL-13	Interleukin-13
IL-33	Interleukin-33
moDC	Monocyte-derived dendritic cell
NKT	Natural killer T-cell
PAMP	Pathogen-associated molecular pattern
PET	Positron emission tomography
PRR	Pattern recognition receptor
RSV	Respiratory syncytial virus
SEV	Sendai virus
TLR3	Toll-like receptor 3

Acknowledgments

I would like to thank first and foremost my dissertation advisor, Dr. Michael Holtzman for not only supporting me as a student, but also pushing me to think critically about my own work, cultivate collaboration with others, and develop independence as a scientist. In addition, I would like to thank my thesis committee, Dr. John Atkinson, Dr. Gaya Amarasinghe, Dr. Mark Miller, Dr. Rodney Newberry, and Dr. Wayne Yokoyama who have provided invaluable advice and guidance to allow me to complete my dissertation project. I would like to thank the numerous members of our laboratory, and in particular Dr. Kangyun Wu and Dr. Yong Zhang, for providing substantial and insightful feedback and technical assistance on my project. I would also like to thank our collaborators: Dr. Marco Colonna, Dr. Yongjian Liu, Dr. Mark Miller, Dr. Andrey Shaw, and Dr. Matthias Mack for providing reagents and expertise that were critical for this project. I would like to thank both the staff and faculty of the Medical Scientist Training Program at Washington University, whose help and efforts have made much of my research and training possible. I would also like to thank the NIH for financial support during my graduate school years. Finally, I would like to thank my parents: my father for inspiring my interest in science, and my mother, whose support has allowed me to get to where I am today and whose loving memory I will carry on with me in the next step of my career.

Xinyu Wang

Washington University in St. Louis

May 2019

Abstract

Activation of Toll-like Receptor 3 Translates to Long-term Post-viral Lung Disease

by

Xinyu Wang

Doctor of Philosophy in Biology & Biomedical Sciences

Immunology

Washington University in St. Louis, 2019

Professor Michael Holtzman, Chair

Chronic obstructive lung disease (COPD) causes substantial human and economic costs both in the US and worldwide. To identify the molecular mechanisms to allow for targeted therapies for COPD, we developed a high-fidelity mouse model of chronic lung inflammation using the natural rodent pathogen Sendai virus (SeV). While nucleic acid-sensing pattern recognition receptors are important for innate immune responses to viral pathogens, there have been few studies investigating their role in the context of chronic disease. Here we show that Toll-like receptor 3 (Tlr3) signaling is required for the development of chronic lung disease in a postviral mouse model. Activation of Tlr3 in inflammatory monocyte-derived dendritic cells (moDCs) is necessary for the development of chronic lung disease. moDCs form an immune cell niche that drives epithelial alveolar type II cell (AT2) proliferation and interleukin-33 (Il33) expression. Il33 then leads to activation of downstream effector immune cells that produce a chronic inflammatory disease phenotype.

Introduction

Chronic obstructive lung disease (COPD) is one of the leading causes of death in the US, behind only cancer and heart disease. As of 2014, an estimated fifteen million people in the US have been diagnosed with COPD, with an annual health care cost of $32 billion, projected to increase to $50 billion by 2020. Despite the substantial human and economic costs associated with COPD, existing therapies using bronchodilators, inhaled corticosteroids, and phophodiesterase-4 inhibitors are often inadequate for treating severe or refractory COPD patients.

COPD, which is broadly defined as irreversible impairment of airflow in the lungs, is staged based on the severity of decrease in forced expiratory volume in one second (FEV_1). COPD often manifests with chronic bronchitis and emphysema, which can over time lead to chronic respiratory failure. Worldwide, smoking is the most frequent cause of COPD, although only 20 – 25% of smokers develop the disease, and those who do vary greatly in disease severity and progression. Furthermore, a fraction of COPD cases cannot be attributed to smoking. (Holtzman et al., 2002; Jackson et al., 2008; Sigurs et al., 2005). Although COPD is a chronic disease that develops in adulthood, recent evidence has emerged suggesting that the origins of COPD may arise much earlier. One early study looking at thousands of individuals in the UK found a very close correlation between childhood respiratory disease and mortality from COPD fifty years later (Shaheen et al. 1995).

Cessation of smoking often does not stop progression of disease. Inflammation in COPD involves self-amplifying loops that lead to persistent mucus cell metaplasia, alveolar apoptosis, and lung remodeling by extracellular matrix proteases. Recruitment of inflammatory cells such neutrophils, macrophages, lymphocytes, and other innate immune cells contribute to lung

dysfunction and alveolar injury.

Bacterial and viral infections are one of the most common causes of COPD exacerbations. RNA viruses such as RSV and influenza can activate PAMPs and lead to inflammatory gene transcription through IRF3/7 and NF-kB. RNA analogs such as polyI:C have been shown to synergize with cigarette smoke to amplify emphysema and airway fibrosis in mice (Kang et al. 2008).

COPD is a complex disease process that is likely a combination of both genetic predispositions and external factors. There is an intricate interplay, much of which is still not well-understood, between lung epithelial cells and immune cells, that allow for exposure to stimuli such cigarette smoke and respiratory viruses to cause the development of chronic disease. Identifying both the critical timing window during which this disease process sets in as well as the pathologic mechanisms that lead to it is essential to developing targeted therapies.

Modeling Acute and Chronic Airway Disease in Mice

Role of iNKT cells and macrophages in chronic airway disease

To identify the pathologic mechanisms that would allow for more directed therapeutic intervention, we have developed a high-fidelity mouse model of chronic lung inflammation. In this model, a natural rodent pathogen that is known as Sendai virus (SeV) is used in place of the human pathogen (RSV). SeV is able to replicate efficiently in mice and produce both severe acute illness and subsequent chronic obstructive lung disease that is typical of the pathologic process found in humans (Walter et al., 2002). The acute illness is characterized by an increase in viral titers that peaks between 3 and 5 days post-infection (dpi), along with accompanying loss of body weight. Monocytic and neutrophilic inflammation is prominent during this time period but by 7 dpi, the virus is mostly

cleared as a result of the adaptive immune system, and animals are able to recover their weight. However, animals begin developing chronic lung pathology after 21 dpi and by 49 dpi, there is pronounced mucus cell metaplasia of the large airways, inflammatory cell infiltrate, neo-bronchiolization, and airway hyper-reactivity, all characteristic of COPD symptoms in humans. Furthermore, this disease never seems to resolve and persists for the lifetime of the animal.

In previous work using this model system, we determined that postviral airway disease depends on the persistent activation of an innate immune axis wherein invariant natural killer T (iNKT) cells direct lung macrophages towards Il13 production and alternative, or M2 polarization (Table 1. Kim et al., 2008). Both *CD4*$^{-/-}$ and *CD8*$^{-/-}$ mice continued to develop chronic airway disease, but op/op mice or clodronate-treated mice did not. This mechanism for disease was unexpected, since the adaptive immune response was generally thought to underlie chronic inflammatory diseases. More recently, we found that heterozygous mice that carry an osteocalcin-driven *Csf1* transgene (*wt/opT*) showed a reduction in lung monocyte-macrophage populations at 49 dpi that correlated with reduced induction of Il13 expression and mucus cell metaplasia. Survival of lung macrophages depended on the production of soluble Trem2 protein (sTrem2) (Wu et al. 2015). This innate immune axis also appears relevant to human disease since increased numbers of invariant NKT (iNKT) cells and Il13-expressing M2 macrophages are found in the lungs of humans with severe asthma or COPD (Agapov et al., 2009; Byers and Holtzman, 2010; Chupp et al., 2007; Molet et al., 2005).

Role of epithelial cells in development of lung pathology

Airway epithelial cells (AECs) are one of the first cells to respond to environmental stimuli and studies have shown that they play an important role in mediating immune cell infiltration in

asthma and COPD (Walter et al. 2001, Byers et al. 2013). AECs express a broad arrangement of pattern recognition receptors such as the Toll-like receptors (TLRs), RIG-I-like receptors (RLRs) and NOD-like receptors (NLRs). Exposure to allergens, cigarette smoke, or nucleic acids from viruses can activate downstream signaling leading to expression of interferon-stimulated genes and inflammatory cytokines. Recent studies have shown that a basal progenitor population of AECs upregulate expression of Il33 after viral infection, which in turn can drive Il13 expression that contributes to chronic lung inflammation (Brett et al. 2013). Il33 expression is also increased in patients with COPD, which supports this hypothesis.

Identifying how epithelial and immune cell PRR activation interact and lead to the development of chronic airway disease is critical for developing targeted therapies. In this study we seek to characterize in detail the effect of one such PRR, Toll-like receptor 3 (Tlr3), and its role on the driving viral-induced long-term lung disease.

Tlr3 expression and signaling

Tlr3 was first identified as a sensor for the double-stranded RNA analog polyI:C and induced both NF-kB-mediated gene expression and type I interferons (Alexopoulou et al. 2001). Furthermore, Tlr3 was found to have distinct roles compared to the dsRNA-activated kinase PKR. PKR was found to be important for sensing cytoplasmic RNA from viral infection whereas Tlr3 was important for sensing extracellular RNA (Carpentier et al. 2007). In unstimulated cells, Tlr3 is located in the endoplasmic reticulum, where UNC-93b regulates its trafficking to the endosome. Acidification of endosomes is required for Tlr3 dimerization, and subsequent phosphorylation of Tyr^{759} and Tyr^{858} located on the cytoplasmic domain (Wang et al. 2010, Kim et al. 2008, de Bouteiller et al. 2005). Tyrosine phosphorylation is required for recruiting Toll-interleukin-1 receptor domain-

containg adaptor protein interferon-B (Trif), the adaptor protein that mediates downstream signaling (Sakar et al. 2007). Recent studies have also suggested the Tlr3 can be phosphorylated by c-Src, epidermal growth factor receptor (Egfr), phosphoinositide 3-kinase (PI3K), and Bruton's tyrosine kinase (Btk) (Johnson et al. 2006, Yamashita et al. 2012, Sun et al. 2012, Lee et al. 2012). However, the role of these kinases in mediating Tlr3 signaling still needs to be elucidated.

Trif associates in a complex with tumour necrosis factor receptor-associated factor 3 (Traf3), Traf family member-associated with NFkB activation binding kinase (Tbk1) and IkB kinase e (IKKe), which leads to IRF-mediated gene transcription. Trif also recruits protein kinase receptor-interaction protein 1 (RIP1) and Traf6, which in turn recruit Tab2, Tab3, and Tak1 to mediate activation of the IKK complex and MAPK pathway. Thus, Tlr3 signaling through Trif can result in type I IFN production through Irf3, inflammatory gene transcription through NFkB and AP-1, and cell death through Rip1 activation.

Recently, it has been reported that Tlr3 can also signal independently of Trif (Yamashita et al. 2012). Upon binding to dsRNA, Tlr3 was able to signal through the proto-oncogene c-Src, and affected cell migration and proliferation. Another report studying coxsackievirus B3 myocarditis found that Trif-deficient mice had significantly worse disease than Tlr3-deficient mice (Abston et al. 2012).

In addition to being activated by viral replication intermediates, Tlr3 has also been reported to recognize endogenous RNA released from necrotic cells and thus may function as a damage-associated molecular pattern recognition receptor (Kariko et al. 2004, Cavassani et al. 2008). Interestingly, human patients with genetic deficiency of Tlr3 are more susceptible to herpes simplex virus 1 (HSV-1)-induced encephalitis, suggesting that Tlr3 has a non-redundant function in controlling HSV-1 infection in the CNS.

Deletion of Tlr3 has been shown to be beneficial in some mouse models of respiratory viral infections. *Tlr3*$^{-/-}$ mice had decreased acute inflammatory response to rhinovirus, influenza A (IAV), and respiratory syncitial virus (RSV), suggesting that Tlr3 may contribute to over-activation of pro-inflammatory genes after viral infection (Wang et al. 2011, Le Goffic et al. 2006, Groskreutz et al. 2006).

The objective of this dissertation is to identify the role Tlr3 plays in mediating both the acute and chronic inflammatory response to SeV. By understanding the immunologic mechanism and critical timing window by which a beneficial antiviral inflammatory response can be transformed into a pathologic one, we hope to be able to highlight pathways that will allow for developing novel therapies for the treatment of COPD.

Summary of Chapters

Chapter 1: Characterization and identification of immune pathways leading to chronic lung disease in Tlr3-deficient animals

a. Characterization of chronic lung inflammation in Tlr3-deficient animals

b. Characterization of chronic lung inflammation in Trif-deficient animals

Chapter 2: Understanding the mechanism by which acute inflammatory cells contributes to chronic disease

a. Investigating the role of Tlr3 on recruiting inflammatory immune cells

b. Investigating the role of monocyte-derived dendritic cells on chronic lung disease

Chapter 1: Characterization and Identification of Immune Pathways Leading to Chronic Lung Disease in Tlr3-deficient Animals

Tlr3 deficiency results in reduced chronic lung disease

Due to previous work in our lab that highlighted the importance of innate immune-driven pathology in chronic lung disease after viral infection, we asked whether Tlr3 deficiency affected the development of chronic postviral lung disease. We found that chronic lung inflammation was markedly attenuated in *Tlr3*$^{-/-}$ mice compared to wildtype control mice, with decreased induction of Il13 gene expression at 49 dpi, reduced mucus cell metaplasia (reflected in decreased Muc5ac gene expression and immunostaining in the airway epithelium) and reduced alternative polarization of lung macrophages as evidenced by decreased levels of Arg1 gene expression (Fig. 1a). *Tlr3*$^{-/-}$ mice also had significantly decreased levels of Il33 expression relative to WT controls at both the mRNA and protein level (Fig. 1b). Il33 has previously been shown to be a critical cytokine upregulated in lung epithelial cells after SeV infection that drives downstream inflammatory immune cell function (Byers et al. 2013). To ask whether the difference in our observed Il33 expression was localized to epithelial cells, we sorted lung epithelial cells using flow cytometry (Fig. 1c) and compared levels of Il33 in the epithelial compartment to the immune and endothelial compartments. We found that Il33 in wildtype mice was exclusively increased in the epithelial compartment at 49 dpi, consistent with prior published results, and that this increase did not occur in *Tlr3*$^{-/-}$ mice (Fig. 1d). On histology, *Tlr3*$^{-/-}$ mice also had significantly decreased lung pathology relative to WT controls at 49 dpi, as evidenced by decreased PAS positivity, hematoxylin signal, and Muc5ac immunostaining (Fig. 1e, f). In contrast, Tlr7, Tlr9, and Mda5 deficiency had no significant effect on the development of chronic lung disease, despite the fact that these three PRRs are also activated by viral nucleic acids

(Fig. S1). These results indicate that Tlr3 has a unique function in the development of chronic lung disease that is not shared with other viral PRRs.

Tlr3 is not necessary for mounting an antiviral response to SeV, but plays a role in recruiting acute inflammatory cells to the lung.

We next asked whether Tlr3 affected the acute antiviral and inflammatory response to SeV infection. We found that *Tlr3*$^{-/-}$ mice had significantly less body weight loss after viral infection, though the peak body weight loss which occurs at 7-8 dpi was similar to WT controls (Fig. 2a). Tlr3 deficiency had no effect on viral titers after SeV infection (Fig. 2b) or on induction of type I interferons and expression of interferon inducible genes (Fig. 2c).

Histologically, *Tlr3*$^{-/-}$ mice displayed less inflammation after infection, with fewer cells infiltrating into the airways at 5 dpi as evidenced by decreased hematoxylin staining relative to WT controls (Fig. 3a, b). Lung DCs can be divided into two subtypes: conventional dendritic cells (cDCs) which arise from a common DC precursor, and monocyte-derived DCs (moDCs), which arise from tissue monocytes. cDCs are further divided into Batf3-dependent CD103^{+} cDCs and Irf4-dependent CD11b^{+} cDCs. Like cDCs, moDCs are characterized by their surface expression of CD11c and CD11b, but unlike cDCs, they also express the macrophage marker CD64. We found that at baseline, moDCs were a rare population the lung, but they were rapidly increased after SeV infection and peak at 12 dpi (Fig. 3c). CD11b^{+} cDCs and CD103^{+} DCs were also increased after infection, but they made up a far lower fraction of the overall DC population compared to moDCs.

Inflammatory myeloid cells have been previously reported to express Ccr2 and to better study this, we analyzed myeloid populations in *Cx3cr1*$^{GFP/+}$/*Ccr2*$^{RFP/+}$ reporter mice at 12 dpi. We

found that lung moDCs, $CD11b^+$ cDCs, and monocytes strongly express both Ccr2 and Cx3cr1 while neutrophils and alveolar macrophages do not express these receptors (Fig. 3d). To study whether there were decreased numbers of Ccr2-positive cells, we developed a ^{64}Cu-labeled peptide that binds specifically to Ccr2 (ECL1i) to allow us to track recruitment of cells that express Ccr2 into the lung using positron emission tomography. We found that while Ccr2 signal in wildtype mice peaked at 12 dpi, the increase was much lower in *Tlr3*$^{-/-}$ mice at this time point (Fig. 3e).

Trif deficiency does not ameliorate chronic lung disease

Most of the published literature has reported Trif as being the primary downstream adapter protein for Tlr3, and unlike other TLRs, Tlr3 is not known to signal through MyD88. As a result, it was surprising when we found that Trif deficiency resulted in a very different outcome in the development of chronic lung disease compared to Tlr3 deficiency.

Acutely, *Trif*$^{-/-}$ mice showed no difference in weight loss or viral titers after SeV infection compared to wildtype animals (Fig. 4a, b). Unlike *Tlr3*$^{-/-}$ mice, *Trif*$^{-/-}$ mice did not show any decrease in inflammatory cell infiltration relative to WT controls at 5 dpi as evidenced by hematoxylin staining (Fig. 4c, d). Using ^{64}Cu-labeled Ccr2 peptide, we were able to compare the intensity of Ccr2 signal in the lungs of *Trif*$^{-/-}$ to *Tlr3*$^{-/-}$ animals at 12 dpi. *Tlr3*$^{-/-}$ animals showed a signal reduction in signal intensity in the lung as we had shown previously, but *Trif*$^{-/-}$ mice did not (Fig. 4e). Furthermore, we did not see a reduction in lung myeloid populations at 12 dpi by flow cytometry (Fig. 4f). At 49 dpi, *Trif*$^{-/-}$ mice showed no reduction in levels of Il13, Muc5ac, or Il33 expression compared to WT mice (Fig. 4g). Similarly on histology, *Trif*$^{-/-}$ mice did not show any reduction in PAS or hematoxylin signal in the lung at 49 dpi (Fig. 4h, i). These results indicate that the inflammatory effect of Tlr3 was not mediated through Trif signaling.

Chapter 2: Understanding the Mechanism by which Acute Inflammatory Cells Contribute to Chronic Disease

Tlr3 expression is upregulated on multiple lung myeloid populations after viral infection, and Tlr3 expression on monocyte-derived dendritic cells.is critical for driving chronic lung disease

Inflammatory monocytes recruited during acute tissue inflammation can differentiate into resident macrophages or dendritic cells. To ask where Tlr3 is expressed, we sorted lung DC and macrophage populations from SeV-UV treated and SeV-infected wildtype mice (Fig. 5a). We found that baseline Tlr3 expression in SeV-UV treated mice was highest in $CD103^+$ DCs, though at 5 dpi, Tlr3 was most significantly upregulated in tissue monocytes, moDCs, and $CD11b^+$ DCs. Interestingly, epithelial cells also showed an increase in Tlr3 mRNA levels at 5 dpi (Fig. 5b). Staining for intracellular Tlr3 protein showed a consistent pattern to mRNA levels (Fig. 5c). In all the cell populations we studied, Tlr3 expression returned to baseline levels after 12 dpi, suggesting that the increase at 5 dpi was primarily an acute response to viral infection.

To investigate whether moDCs had a functional role in the pathogenesis of chronic disease, we adoptively transferred primary lung moDCs from donor mice into recipient *Tlr3*$^{-/-}$ mice. To obtain sufficient numbers of DCs, we sorted cells from the lungs of donor mice at 12 dpi. Recipient mice received $1*10^6$ cells intranasally and were infected with SeV 24 hrs after adoptive transfer. Lungs were then analyzed at 49 dpi for the development of chronic lung disease (Fig. 6a). Adoptive transfer of wildtype moDCs into *Tlr3*$^{-/-}$ mice was able to reconstitute chronic lung disease as evidenced by restoration of PAS and hematoxylin signal (Fig. 6b, c) as well Muc5ac immunostaining at 49 dpi to levels comparable to wildtype control mice that were given intranasal PBS (Fig. 6d, e).

Interestingly, transfer of *Tlr3*$^{-/-}$ moDCs was not able to restore chronic lung disease, suggesting that Tlr3 expression on moDCs was necessary for their functional activation.

Bone marrow-derived dendritic cells (BMDCs) generated in vitro using GM-CSF have been reported to functionally resemble moDCs. To ask whether BMDCs could also reconstitute chronic disease in *Tlr3*$^{-/-}$ mice, we cultured BMDCs from uninfected WT and *Tlr3*$^{-/-}$ donor mice, and transferred them to *Tlr3*$^{-/-}$ recipients a day before SeV infection (Fig. 7a). Transfer of BMDCs showed a similar effect to primary moDC transfer, and WT cells were able to restore chronic lung disease while *Tlr3*$^{-/-}$ cells were not (Fig. 7b, c).

To ask whether transfer of tissue monocytes, the precursor cell to moDCs, could also restore chronic disease in *Tlr3*$^{-/-}$ mice, we compared the effect of transferring primary moDCs sorted from donor mice at 12 dpi to primary tissue monocytes sorted from the same donor mice at 12 dpi. Lungs of recipient mice were analyzed at 21 dpi, which is an earlier timepoint in the development of chronic postviral disease. Surprisingly, while transfer of WT moDCs was able to restore PAS and hematoxylin signal in the lungs of *Tlr3*$^{-/-}$ recipient mice, transfer of WT tissue monocytes was not, suggesting that differentiation into moDCs before transfer was necessary in order to have a functional effect on the development of chronic disease (Fig. 8a, b).

We showed earlier that both tissue monocytes and moDCs expressed surface Ccr2. We assessed whether deletion of Ccr2, which would block recruitment of these cells into the lung, would affect disease outcome. We infected *Ccr2*$^{-/-}$ mice with SeV and found that tissue monocyte recruitment at 5 dpi was almost completely absent (Fig. 9a). However, *Ccr2*$^{-/-}$ mice lost significantly more body weight than control animals and exhibited increased mortality to SeV infection. (Fig. 9b). We found a similar effect on survival using a previously characterized Ccr2-blocking antibody (MC-21) between infection and 5 dpi (data not shown). This suggested that at least some Ccr2-positive

cells are needed for adequate control of viral replication and the complete absence of these cells was detrimental to survival. Given that Ccr2 is also expressed on DCs, NK cells, and T cells (Kim et al. 2001, Egan et al. 2009, Hohl et al. 2009), it is possible that the inability to recruit these cells delays the adaptive response, and causes problems in clearing the virus. This is supported by the fact that both antibody treated mice and *Ccr2*$^{-/-}$ mice continue to lose weight after 7 dpi, but wildtype mice are able to recover (Fig. 9c). In contrast, *Tlr3*$^{-/-}$ mice do not have increased weight loss or mortality after SeV infection and only specific myeloid subsets which may be dispensable for viral clearance are decreased in these mice.

Monocyte-derived dendritic cells directly induce AT2 cell proliferation in vivo

Given that epithelial cell-derived Il33 is decreased in *Tlr3*$^{-/-}$ mice, and evidence that Il33 expression is predominantly localized to type II alveolar cells (AT2) (Byers et al. 2013, Llop-Guevara et al. 2014), we asked whether *Tlr3*$^{-/-}$ deficiency affected AT2 cell numbers after SeV infection using surfactant protein C (Sftpc) staining. In WT controls, AT2 cell counts decreased at 5 dpi, reflecting apoptosis/lysis from viral infection. However, AT2 cells were repopulated by 21 dpi and substantially increased at 49 dpi. Interestingly, this increase did not occur in *Tlr3*$^{-/-}$ mice, and cell numbers remained near baseline levels even at 49 dpi (Fig. 10a).

To assess whether moDCs played a role in AT2 cell proliferation, we quantified Sftpc staining in *Tlr3*$^{-/-}$ mice that were adoptively transferred with WT or *Tlr3*$^{-/-}$ lung moDCs. Transfer of WT moDCs restored AT2 numbers to WT levels at 49 dpi, while transfer of *Tlr3*$^{-/-}$ moDCs partially restored AT2 cell numbers (Fig. 10b). These results suggest that while moDCs appear to be important in inducing AT2 proliferation, Tlr3 expression in moDCs may be dispensable in that regard and may instead play a role in their functional activation.

To address this issue, we asked whether moDCs could directly induce Il33 expression in airway epithelial cells. We sorted $EpCAM^+$ cells from naïve uninfected WT mice and cultured them ex vivo with moDCs purified from WT or *Tlr3*$^{-/-}$ mice at 12 dpi. We found that while WT moDCs were able to induce upregulation of Il33 expression in this culture system, *Tlr3*$^{-/-}$ moDCs were not able induce significant increases Il33 gene expression in naïve epithelial cells (Fig. 10c).

Discussion

We have shown that Tlr3 is critical for chronic lung disease that develops after viral infection. Tlr3 seems to be a unique PRR in this regard, in that it is dispensable for viral clearance, but instead contributes to a pathological inflammatory response to SeV. This response is mediated by the recruitment of inflammatory monocytes that subsequently differentiate into $CD64^{high}$ $CD11c^{+}$ moDCs, which constitute a large proportion of inflammatory cells by 12 dpi. These moDCs appear to be critical in driving AT2 cell proliferation, and in turn may also directly induce Il33 expression from airway epithelial cells. To our knowledge this is the first observed induction of an innate PRR that drives chronic post-viral lung disease and we have identified a novel immune cell niche that contributes to airway pathology (Fig. 11).

We did not observe an effect of Tlr3 deficiency on type I interferon induction, likely due to functional redundancy between Tlr3 and RLR/MAVS pathways in upregulating antiviral genes. Indeed, other studies have reported that RIG-I, and not Tlr3, is necessary for the antiviral response to Sendai virus. It is difficult to track Tlr3 activation *in vivo*, but recent reports have indicated that Tlr3 can also be activated by endogenous RNA released from necrotic cells (Kariko et al., Cavassani et al.). It is possible that RNA released from the turnover of cells during the acute inflammatory response, as well as replicating virus itself, provides a stimulus to activate Tlr3 signaling. Upregulation of Tlr3 expression on lung myeloid and epithelial cells appears to be transient, peaking at 5 dpi but returning to baseline levels by 12 dpi. Although this does not rule out continued activation of Tlr3 in these cells, expression correlates with the timecourse of viral titer, suggesting that cells are directly responding to SeV infection.

Interestingly, *Trif*$^{-/-}$ mice did not show reduced lung pathology compared to WT controls at 49 dpi and showed no reduction in Muc5ac or Il33 expression. Both *Trif*$^{-/-}$ and *Tlr3*$^{-/-}$ animals used

for this study had been backcrossed to B6 animals for at least ten generations, so the result was not due to a difference in genetic background. Trif-deficiency also affects signaling through Tlr4, and it is unknown how loss of Tlr4 signaling may influence disease progression in our model. Trif has been reported to be a negative regulator of MyD88-dependent activation of dendritic cells (Seregin et al. 2011). Furthermore, it has recently been reported that Tlr3 can signal through a Trif-independent pathway (Yamashita et al. 2012). Thus, there are several possible explanations why the *Trif*$^{-/-}$ phenotype is different from *Tlr3*$^{-/-}$ mice. Our results provide evidence that despite being part of the same signaling pathway, these proteins play very different roles and Trif-deficiency is not functionally synonymous with Tlr3-deficiency in vivo.

Recently it has been reported that Ccl2 expression leads to moDC recruitment in an RSV model (Goritzka et al.) although few studies have looked at the role these cells play in chronic COPD models. In our model, we found that lung moDCs peak at 12 dpi, and may produce a proliferative and/or survival signal to alveolar type II cells. moDCs, also known as Tip-DCs or inflammatory DCs, have also been reported to activate effector CD8 T cells and promote Th2 cell-mediated immunity (Plantinga et al. 2013). Adoptive transfer of moDCs was able to completely reconstitute chronic lung disease in *Tlr3*$^{-/-}$ mice, as well as restore AT2 cell numbers and lung Il33 levels, suggesting a common cellular mechanism. GM-CSF induced BMDCs, which are phenotypically similar to moDCs, were also able to restore mucus cell metaplasia and lung disease in *Tlr3*$^{-/-}$ animals. Transfer of tissue monocytes, however, did not have this effect, suggesting that donor monocytes may not fully differentiate into moDCs once taken out of their microenvironment and transferred into a foreign host. Our results indicate that moDCs are functionally important for the development of chronic disease, but we cannot rule out the potential contribution of other myeloid populations to the development of chronic disease such as CD11b^{+} and CD103^{+} DCs.

Further studies are needed to elucidate how depletion of specific subsets of lung DCs cells influence disease outcome.

Both lung moDCs and GM-CSF cultured BMDCs are heterogeneous populations, and it remains a possibility that there are functional differences among subsets of these cells. Indeed, AT2 cells themselves are also heterogeneous, and there may be a subset of epithelial cells that responds to signals released by the immune cell niche. Future studies using single-cell RNA sequencing to tease apart these populations will be very exciting.

Figures

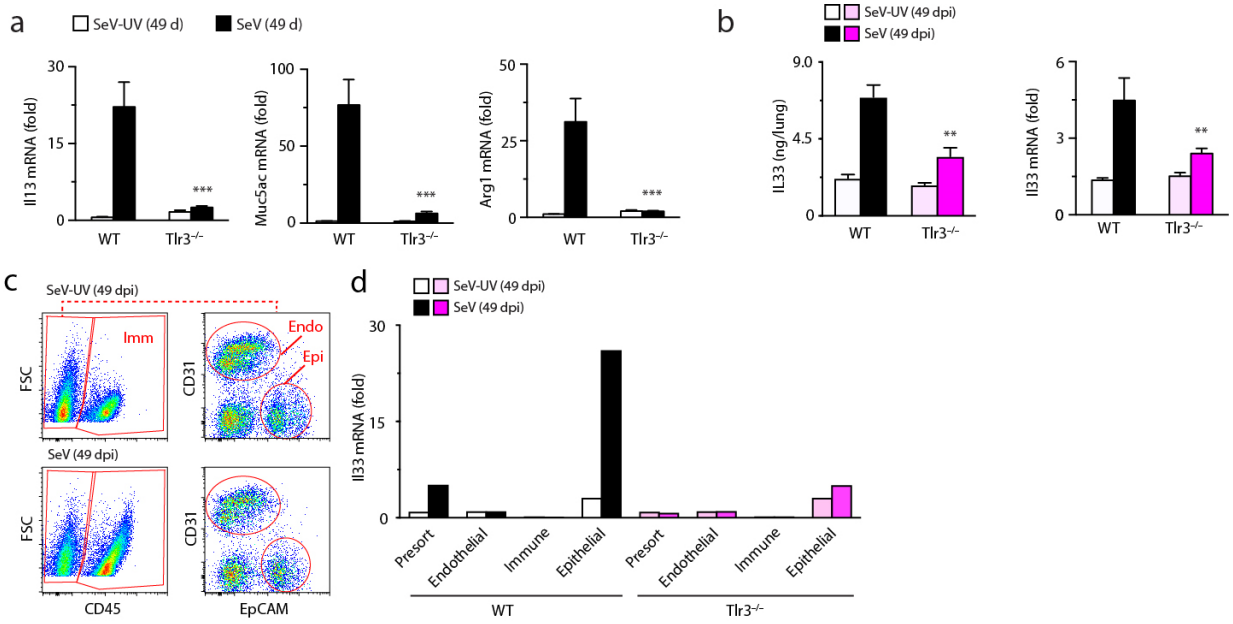
a
SeV-UV (49 d)
SeV (49 d)
Il13 mRNA (fold)
Muc5ac mRNA (fold)
Arg1 mRNA (fold)
WT
Tlr3-/-
b
SeV-UV (49 dpi)
SeV (49 dpi)
IL33 (ng/lung)
Il33 mRNA (fold)
c
SeV-UV (49 dpi)
Imm
Endo
Epi
FSC
CD31
SeV (49 dpi)
CD45
EpCAM
d
Il33 mRNA (fold)
Presort
Endothelial
Immune
Epithelial

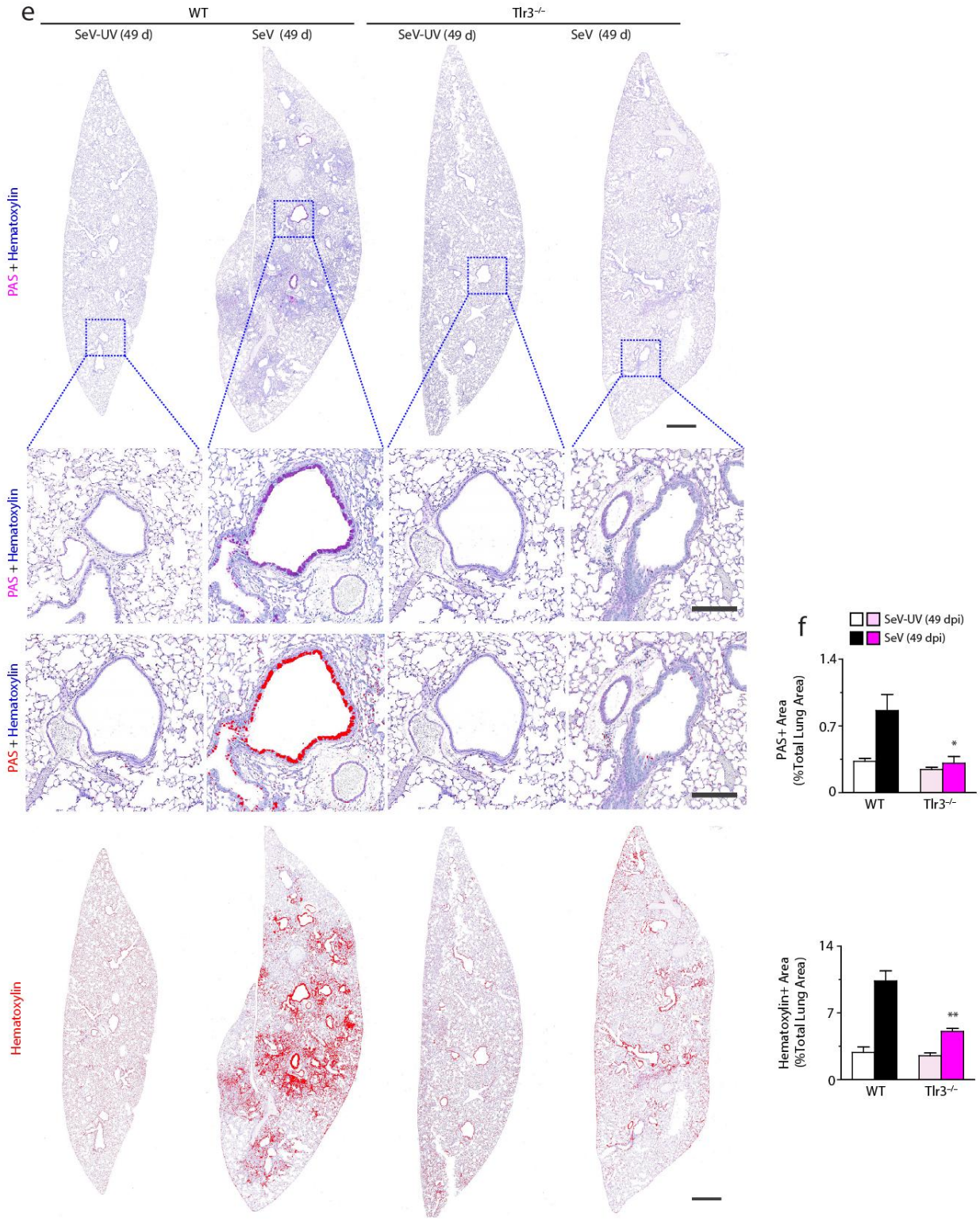
e
WT
Tlr3-/-
SeV-UV (49 d)
SeV (49 d)
SeV-UV (49 d)
SeV (49 d)
PAS + Hematoxylin
PAS + Hematoxylin
PAS + Hematoxylin
Hematoxylin
f
SeV-UV (49 dpi)
SeV (49 dpi)
PAS+ Area (%Total Lung Area)
1.4
0.7
0
*
WT
Tlr3-/-
Hematoxylin+ Area (%Total Lung Area)
14
7
0
**
WT
Tlr3-/-

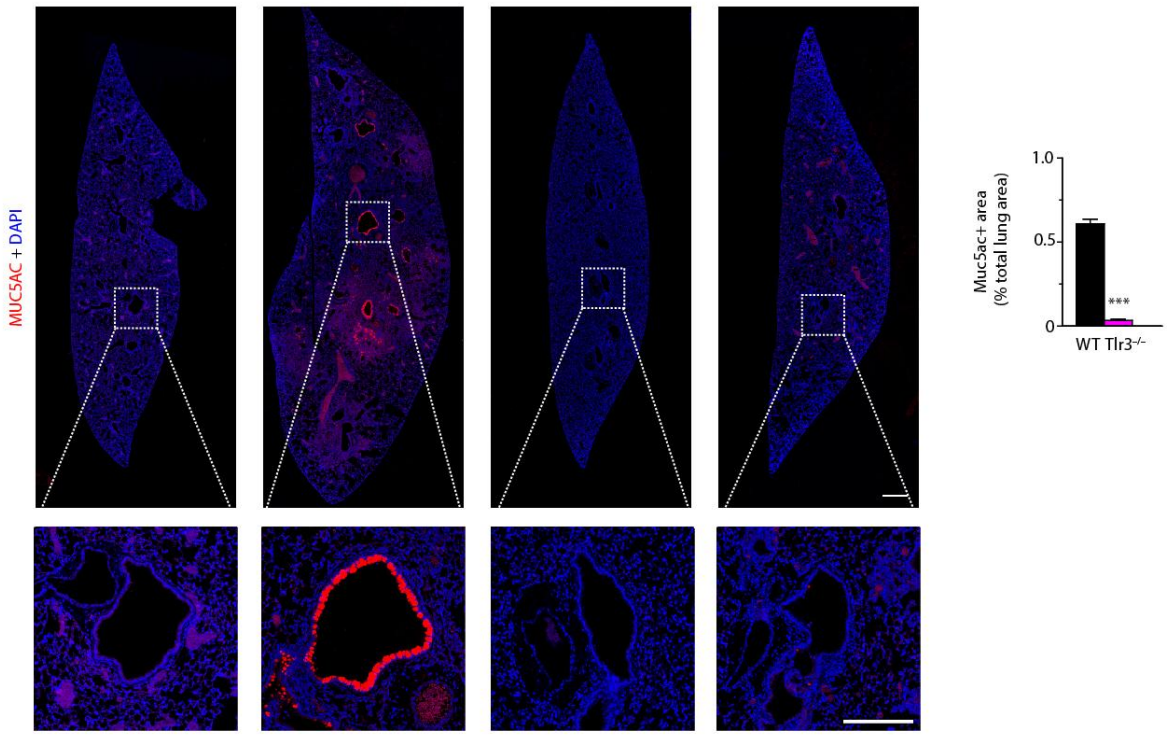

Figure 1

Fig. 1. TLR3 is required for chronic airway disease after viral infection. (**a**) Levels of *Il13*, *Muc5ac*, *and Arg1* mRNA in lungs from wild-type (WT) and *Tlr3*$^{-/-}$ mice at 49 days post-infection (dpi) with SeV or SeV-UV. (**b**) Levels of *Il33* mRNA and protein in lungs from WT and *Tlr3*$^{-/-}$ mice at 49 dpi with SeV or SeV-UV. (**c**) Flow cytometry analysis of EpCAM^{+} epithelial cells, CD31+ endothelial cells, and CD45+ immune cells at 49 dpi with SeV or SeV-UV. (**d**) Levels of *Il33* mRNA in cell populations from (a) in *Tlr3*$^{-/-}$ and WT control mice after infection with SeV or SeV-UV. (**e**) PAS/hematoxylin staining and Muc5ac immunostaining of lungs from WT and *Tlr3*$^{-/-}$ mice at 49 dpi with SeV or SeV-UV. Scale bars = 500 μm (low mag) and 250 μm (high mag). (**f**) Quantification of PAS and colorized hematoxylin staining and Muc5ac immunostaining. For (a-b, e-f), values are mean ± SEM for 5 mice; values are representative of 3 separate experiments.

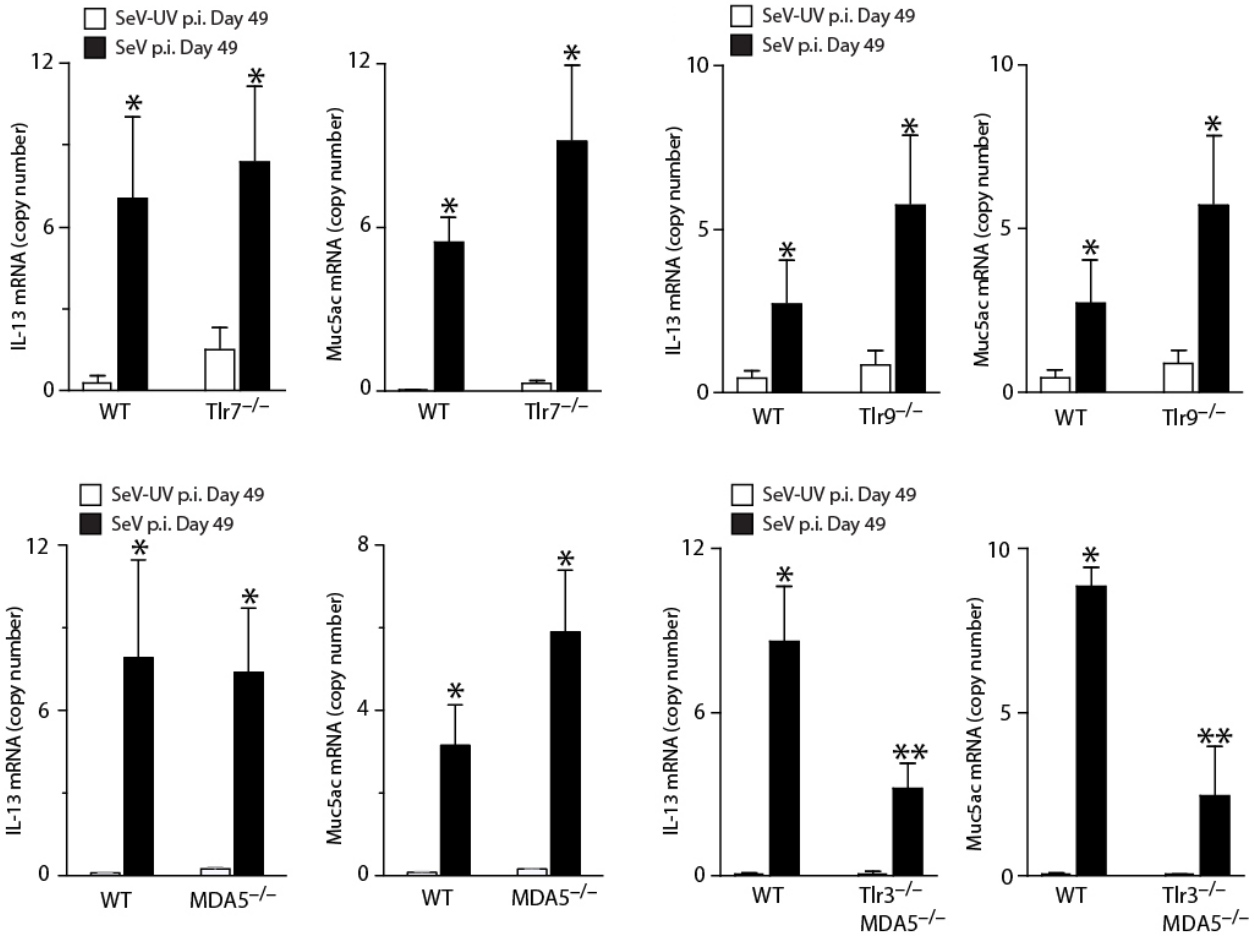

Fig. S1. Effect of other viral PRRs on chronic lung disease. mRNA levels of *Il13* and *Muc5ac* in *Tlr7 -/-, Tlr9-/-, MDA5-/-* and *Tlr3-/--MDA5-/-* double knockout mice. * *P*< 0.05 versus SeV-UV and ** *P*< 0.05 versus WT.

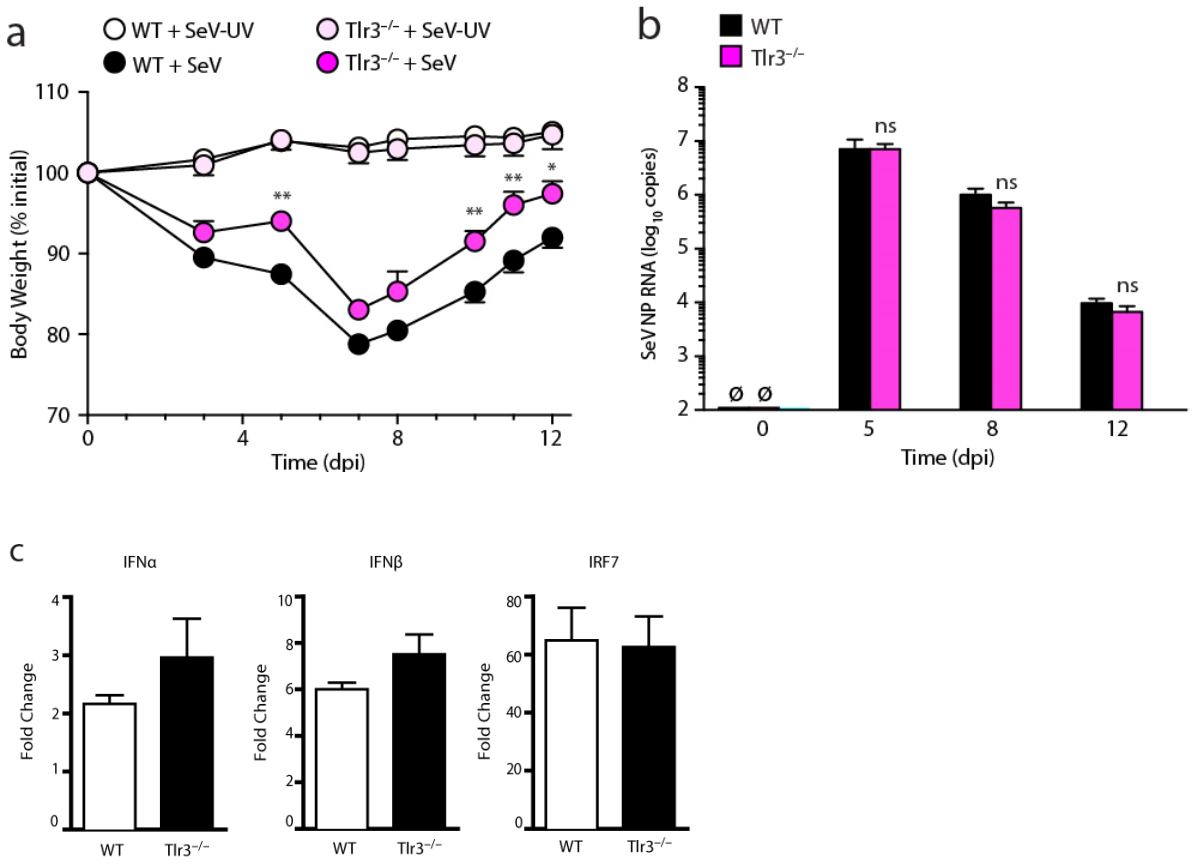

Fig. 2. Effect of Tlr3 on viral replication. (**a**) Body weights from WT and *Tlr3*$^{-/-}$ mice after administration of intranasal SeV and SeV-UV. (**b**) Viral titers at indicated time points after SeV infection from WT and *Tlr3*$^{-/-}$ mice. (**c**) Expression of type I interferons and Irf7 at 3 dpi in WT and *Tlr3*$^{-/-}$ mice. For (a-c), values are mean ± SEM for 5 mice; values are representative of 3 separate experiments.

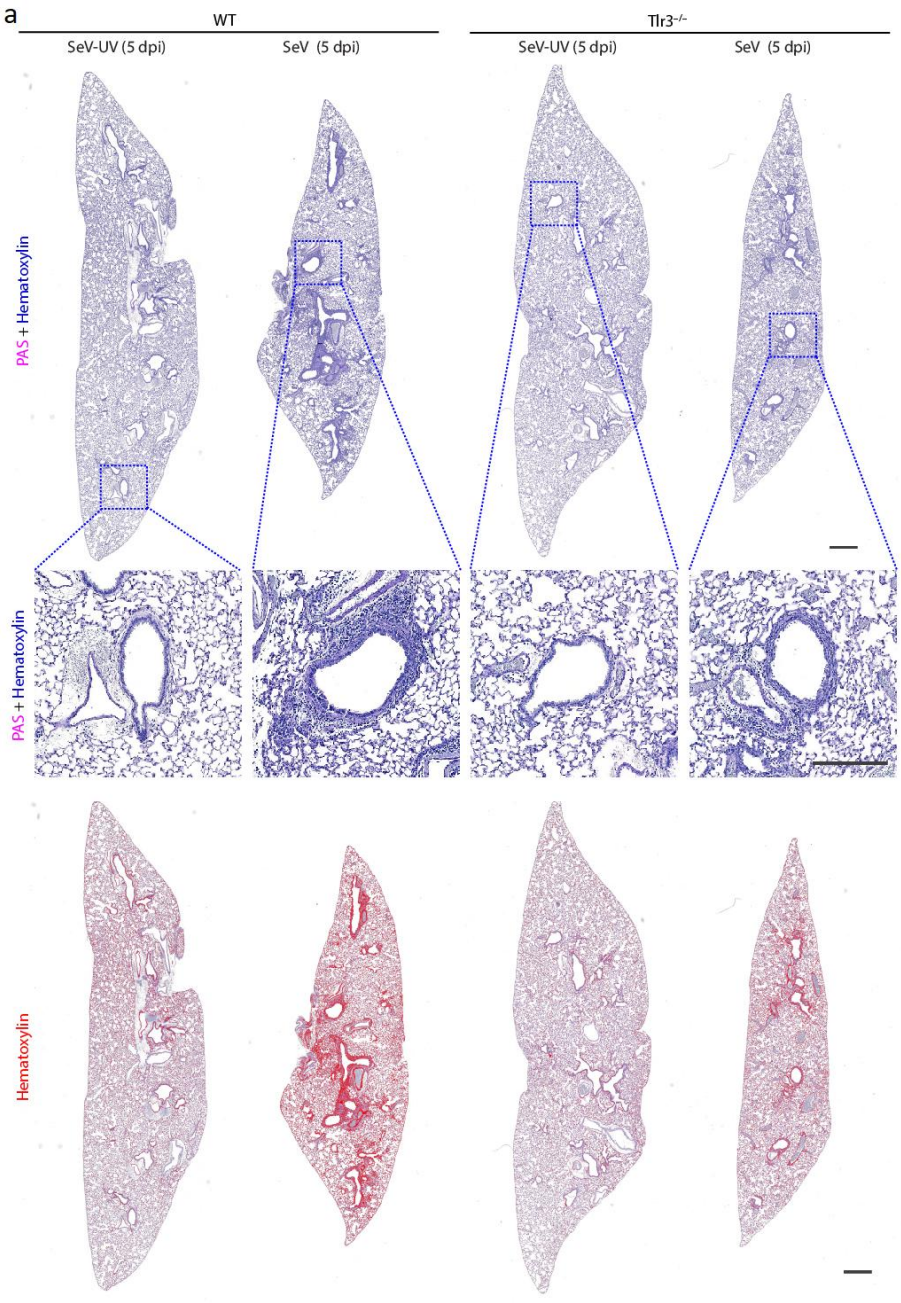
a
WT
Tlr3-/-
SeV-UV (5 dpi)
SeV (5 dpi)
SeV-UV (5 dpi)
SeV (5 dpi)
PAS + Hematoxylin
PAS + Hematoxylin
Hematoxylin

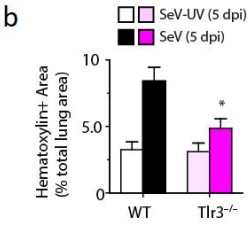
b
SeV-UV (5 dpi)
SeV (5 dpi)
Hematoxylin+ Area
(% total lung area)
10
5.0
0
*
WT
Tlr3-/-

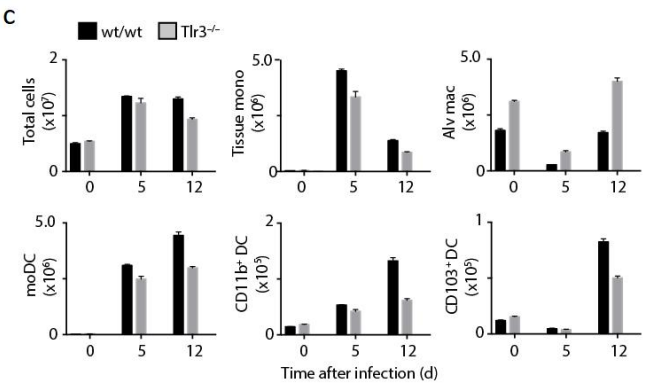
c
wt/wt
Tlr3-/-
Total cells (x10⁷)
Tissue mono (x10⁶)
Alv mac (x10⁶)
moDC (x10⁶)
CD11b+ DC (x10⁵)
CD103+DC (x10⁵)
Time after infection (d)

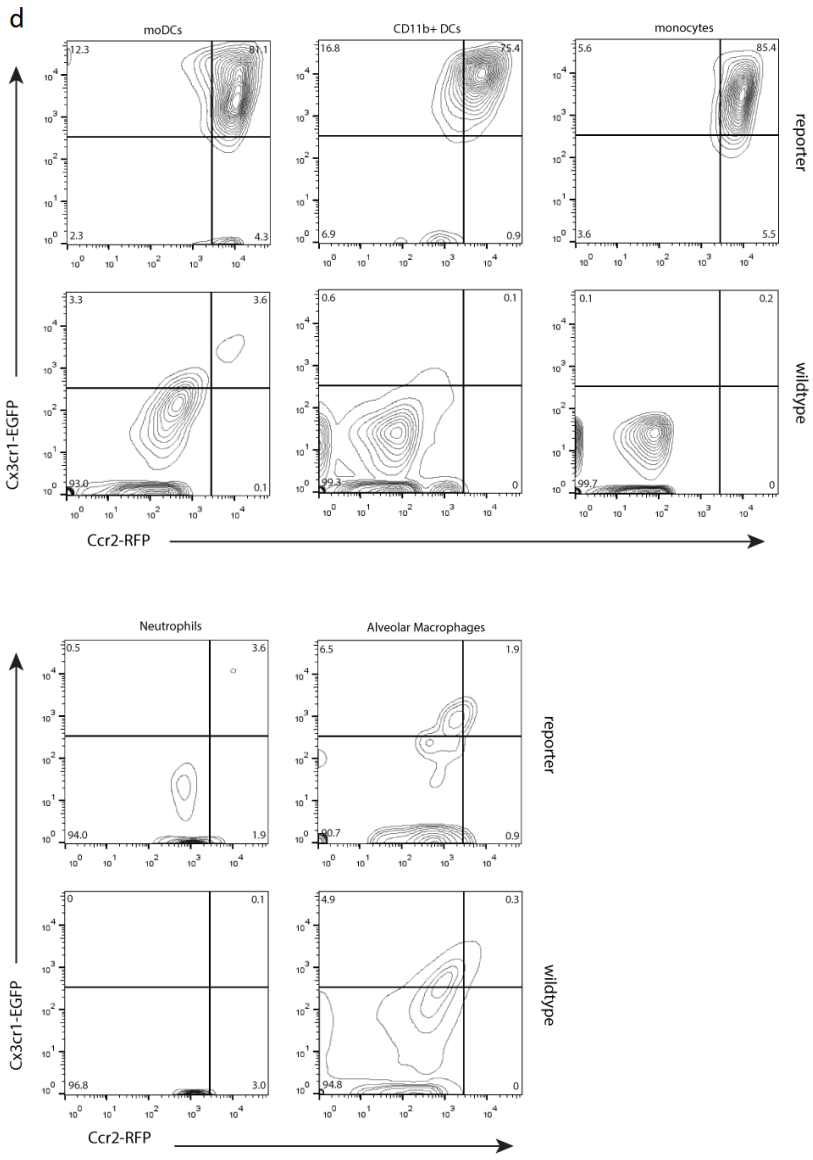
d
moDCs
CD11b+ DCs
monocytes
reporter
wildtype
Cx3cr1-EGFP
Ccr2-RFP
12.3
81.1
2.3
4.3
16.8
75.4
6.9
0.9
5.6
85.4
3.6
5.5
3.3
3.6
93.0
0.1
0.6
0.1
99.3
0
0.1
0.2
99.7
0
Neutrophils
Alveolar Macrophages
0.5
3.6
94.0
1.9
6.5
1.9
90.7
0.9
0
0.1
96.8
3.0
4.9
0.3
94.8
0
e
WT (12 dpi)
Tlr3−/− (12 dpi)
WT
Tlr3−/−
% ID/gram
dpi
5
12
19
47

Fig. 3. Tlr3-mediated acute inflammation. (**a**) Representative PAS/Hematoxylin-stained sections of airway from WT and *Tlr3*$^{-/-}$ mice at 5 dpi with SeV or SeV-UV. Scale bars = 500 μm (low mag) and 250 μm (high mag). (**b**) Quantification of hematoxylin staining. (**c**) Cell counts of myeloid populations from WT and *Tlr3*$^{-/-}$ mice at indicated timepoints. (**d**) Expression of *CX3CR1-EGFP* and *CCR2-RFP* on myeloid populations at 12 dpi on *Cx3cr1*$^{EGFP/+}$/*Ccr2*$^{RFP/+}$ reporter mice compared to wildtype controls and proportion of indicated cell populations as a percent of all *CCR2-RFP* positive cells. (**e**) Axial (top) and contralateral (bottom) PET scans showing lung uptake of ^{64}Cu-labeled peptide (ECL1i) targeted against Ccr2 at 12 dpi. Timecourse of tracer uptake comparing *Tlr3*$^{-/-}$ and wildtype animals is shown on the right. Cell counts from purified whole lung populations at 5 dpi. For (a-c, e), values are mean ± SEM for 3 mice; for (a-c), values are representative of 3 separate experiments.

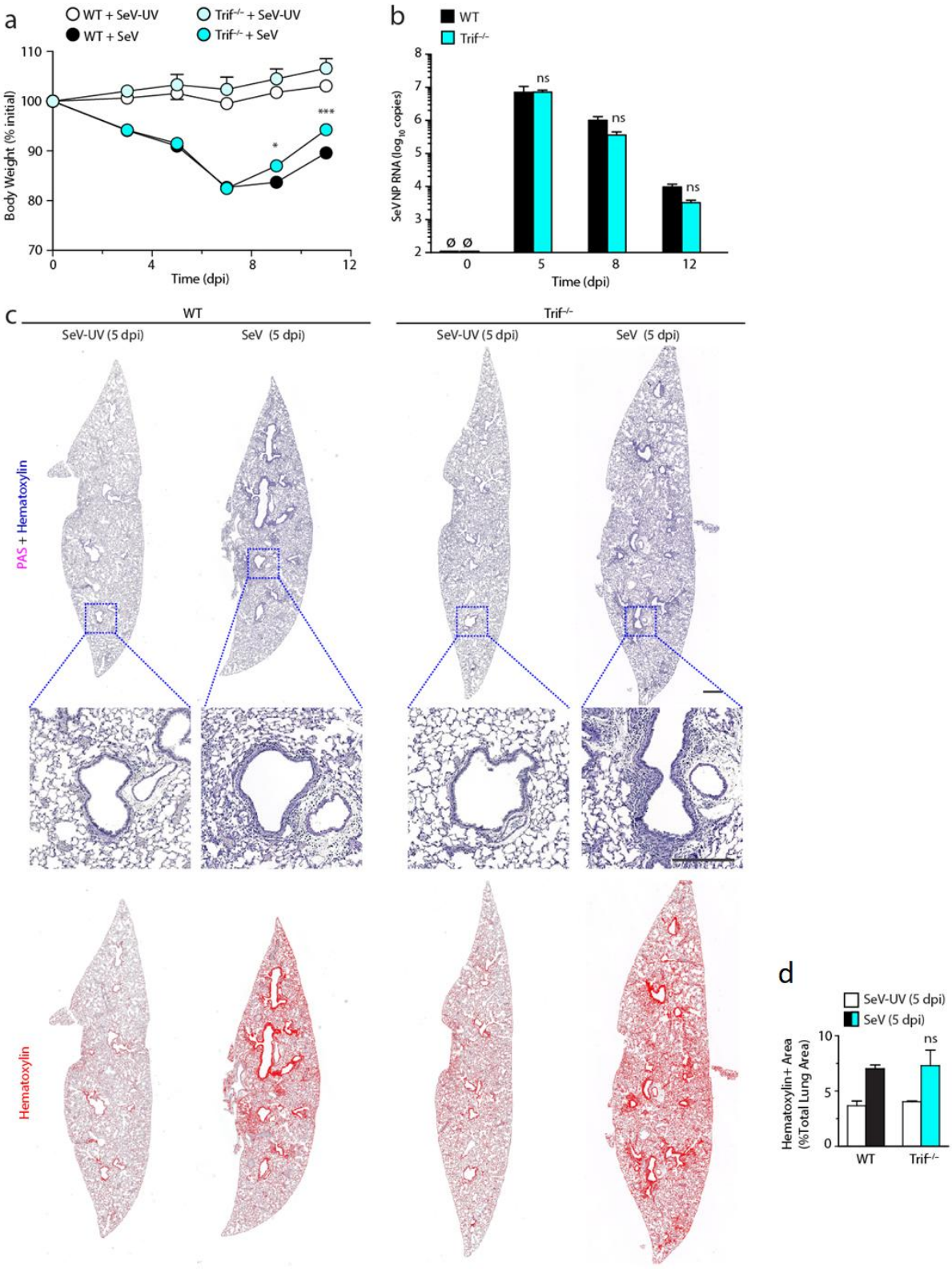
a
WT + SeV-UV
WT + SeV
Trif-/- + SeV-UV
Trif-/- + SeV
Body Weight (% initial)
Time (dpi)
***
*
b
WT
Trif-/-
SeV NP RNA (log10 copies)
ns
Time (dpi)
c
WT
Trif-/-
SeV-UV (5 dpi)
SeV (5 dpi)
PAS + Hematoxylin
Hematoxylin
d
SeV-UV (5 dpi)
SeV (5 dpi)
Hematoxylin+ Area (%Total Lung Area)
ns
WT
Trif-/-

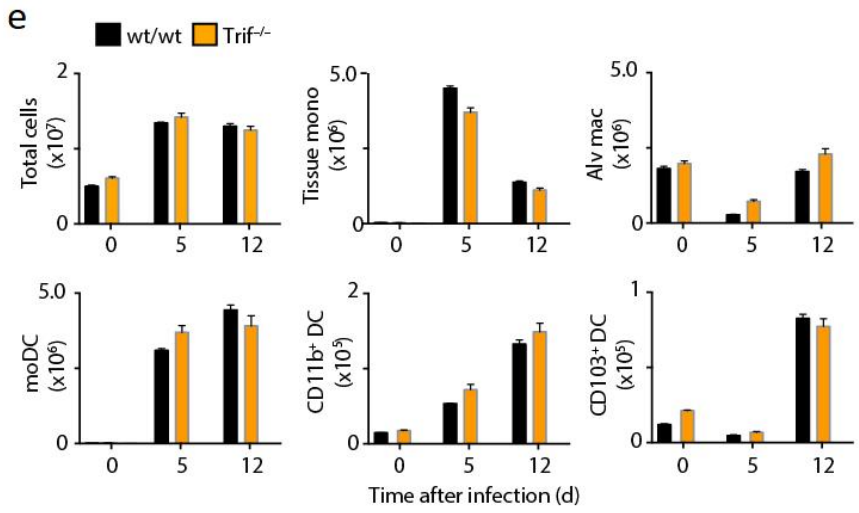
e
wt/wt
Trif-/-
Total cells (x10^7)
Tissue mono (x10^6)
Alv mac (x10^6)
moDC (x10^6)
CD11b+ DC (x10^5)
CD103+ DC (x10^5)
Time after infection (d)

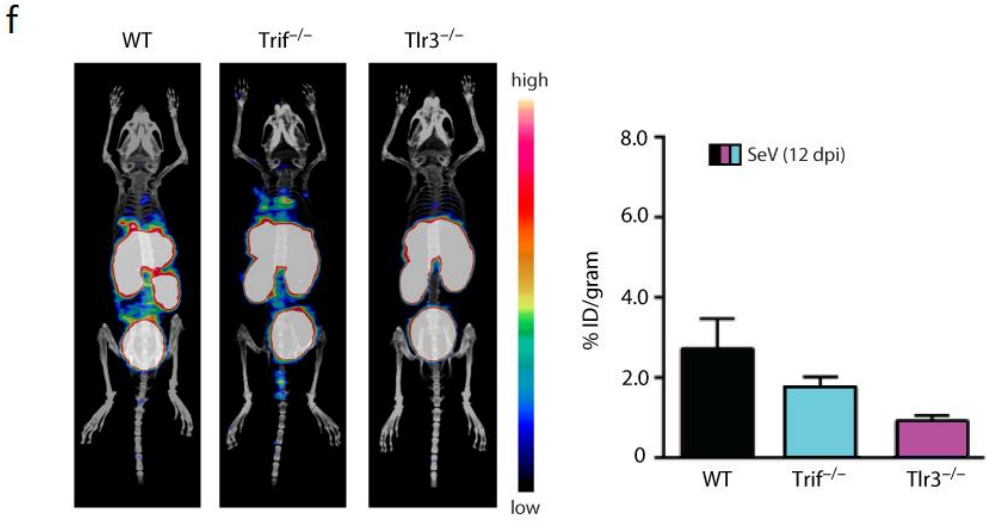
f
WT
Trif-/-
Tlr3-/-
high
low
SeV (12 dpi)
% ID/gram
WT
Trif-/-
Tlr3-/-

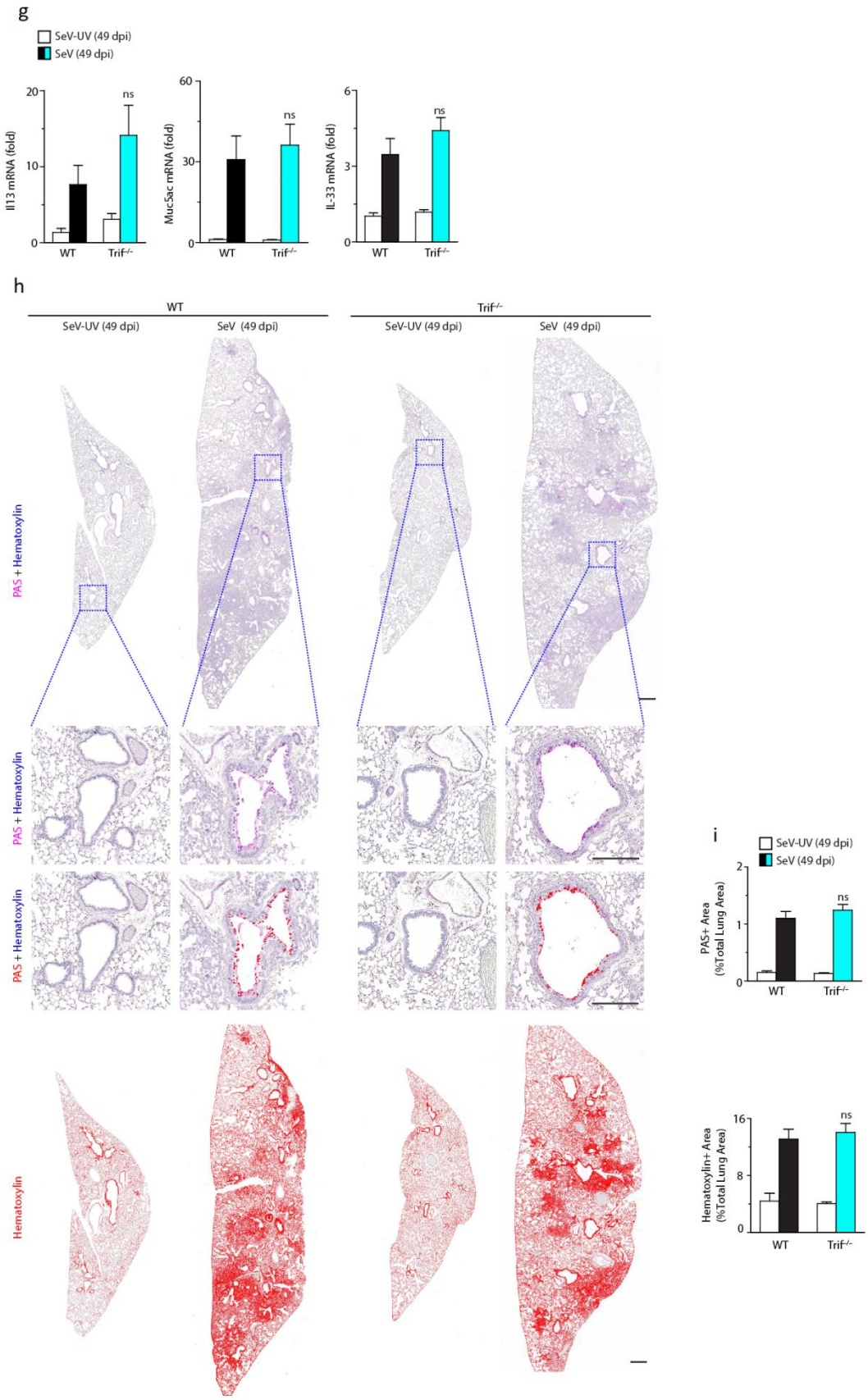
g
SeV-UV (49 dpi)
SeV (49 dpi)
Il13 mRNA (fold)
Muc5ac mRNA (fold)
IL-33 mRNA (fold)
ns
WT
Trif-/-
h
WT
Trif-/-
SeV-UV (49 dpi)
SeV (49 dpi)
PAS + Hematoxylin
Hematoxylin
i
PAS+ Area (%Total Lung Area)
Hematoxylin+ Area (%Total Lung Area)

Fig. 4. TRIF is not required for development of acute or chronic lung disease. (**a**) Body weights for *Trif*$^{-/-}$ and WT control mice after infection with SeV or SeV-UV. (**b**) Levels of SeV *NP* RNA in lungs from the same strains of mice after infection with SeV. (**c**) PAS/Hematoxylin staining of lung sections from the same strains of mice at 5 dpi with SeV or SeV-UV. Scale bars = 500 μm (low mag) and 250 μm (high mag). (**d**) Quantification of colorized hematoxylin staining. (**e**) Flow cytometry counts of immune cell populations at indicated time points. (**f**) PET scans showing lung uptake of ^{64}Cu-labeled peptide (ECL1i) targeted against Ccr2 at 12 dpi. (**g**) Levels of *Il13*, *Muc5ac*, *and Il33* mRNA in lungs from WT and *Trif*$^{-/-}$ mice at 49 days post-infection. (**h**) PAS-hematoxylin staining of lung sections from *Trif*$^{-/-}$ mice at 49 dpi with SeV or SeV-UV. Scale bars = 500 μm (low mag) and 250 μm (high mag) (**i**) Quantification of PAS and colorized hematoxylin staining at 49 dpi from (h). For (a-g), values are mean ± SEM for 5 mice; for (h) photos are representative of 3 separate experiments.

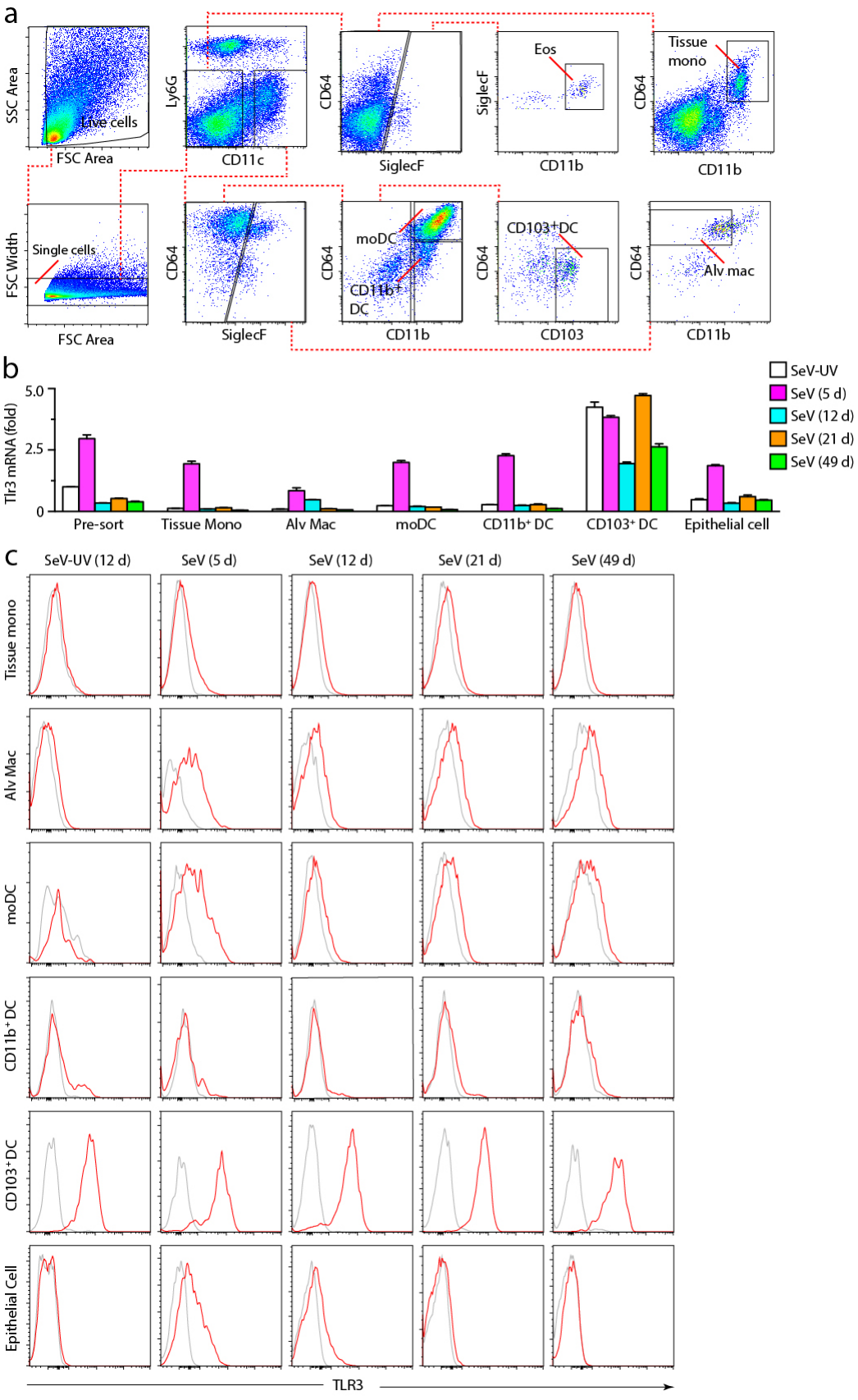
a
SSC Area
FSC Area
Live cells
Ly6G
CD11c
CD64
SiglecF
Eos
SiglecF
CD11b
Tissue mono
CD64
CD11b
FSC Width
FSC Area
Single cells
CD64
SiglecF
moDC
CD11b+ DC
CD64
CD11b
CD103+DC
CD64
CD103
Alv mac
CD64
CD11b
b
Tlr3 mRNA (fold)
5.0
2.5
0
Pre-sort
Tissue Mono
Alv Mac
moDC
CD11b+ DC
CD103+ DC
Epithelial cell
SeV-UV
SeV (5 d)
SeV (12 d)
SeV (21 d)
SeV (49 d)
c
SeV-UV (12 d)
SeV (5 d)
SeV (12 d)
SeV (21 d)
SeV (49 d)
Tissue mono
Alv Mac
moDC
CD11b+DC
CD103+DC
Epithelial Cell
TLR3

Fig. 5. Site of Tlr3 expression and activation after viral infection. (**a**) Flow cytometry analysis of lung myeloid cell populations (tissue monocytes (Tissue mono), moDCs, $CD11b^+$ DCs, CD103+DCs, alveolar macrophages (Alv mac), eosinophils, and epithelial cells) in WT and *Tlr3*$^{-/-}$ mice after infection with SeV-UV or SeV. (**b**) Levels of *Tlr3* mRNA for cell populations from (a) at indicated times after SeV infection. (**c**) Flow cytometry analysis of intracellular Tlr3 for cell populations from (a) at indicated times after SeV infection. For (b), values are mean ± SEM for 5 mice. * $P < 0.05$ versus SeV-UV.

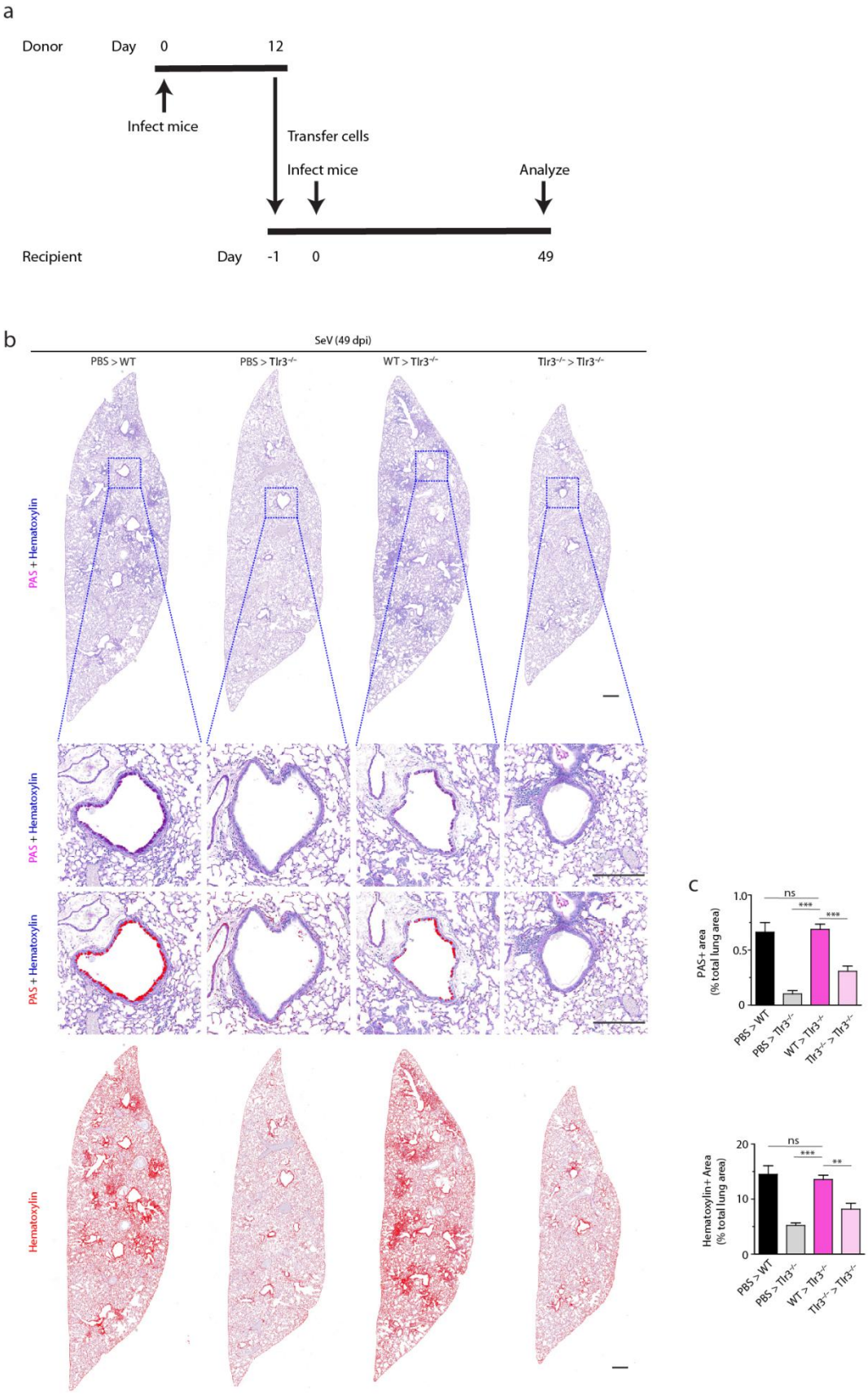
a
Donor
Day
0
12
Infect mice
Transfer cells
Infect mice
Analyze
Recipient
Day
-1
0
49
b
SeV (49 dpi)
PBS > WT
PBS > Tlr3-/-
WT > Tlr3-/-
Tlr3-/- > Tlr3-/-
PAS + Hematoxylin
PAS + Hematoxylin
PAS + Hematoxylin
Hematoxylin
c
PAS+ area (% total lung area)
1.0
0.5
0
ns
***
***
PBS > WT
PBS > Tlr3-/-
WT > Tlr3-/-
Tlr3-/- > Tlr3-/-
Hematoxylin+ Area (% total lung area)
20
10
0
ns
***
**
PBS > WT
PBS > Tlr3-/-
WT > Tlr3-/-
Tlr3-/- > Tlr3-/-

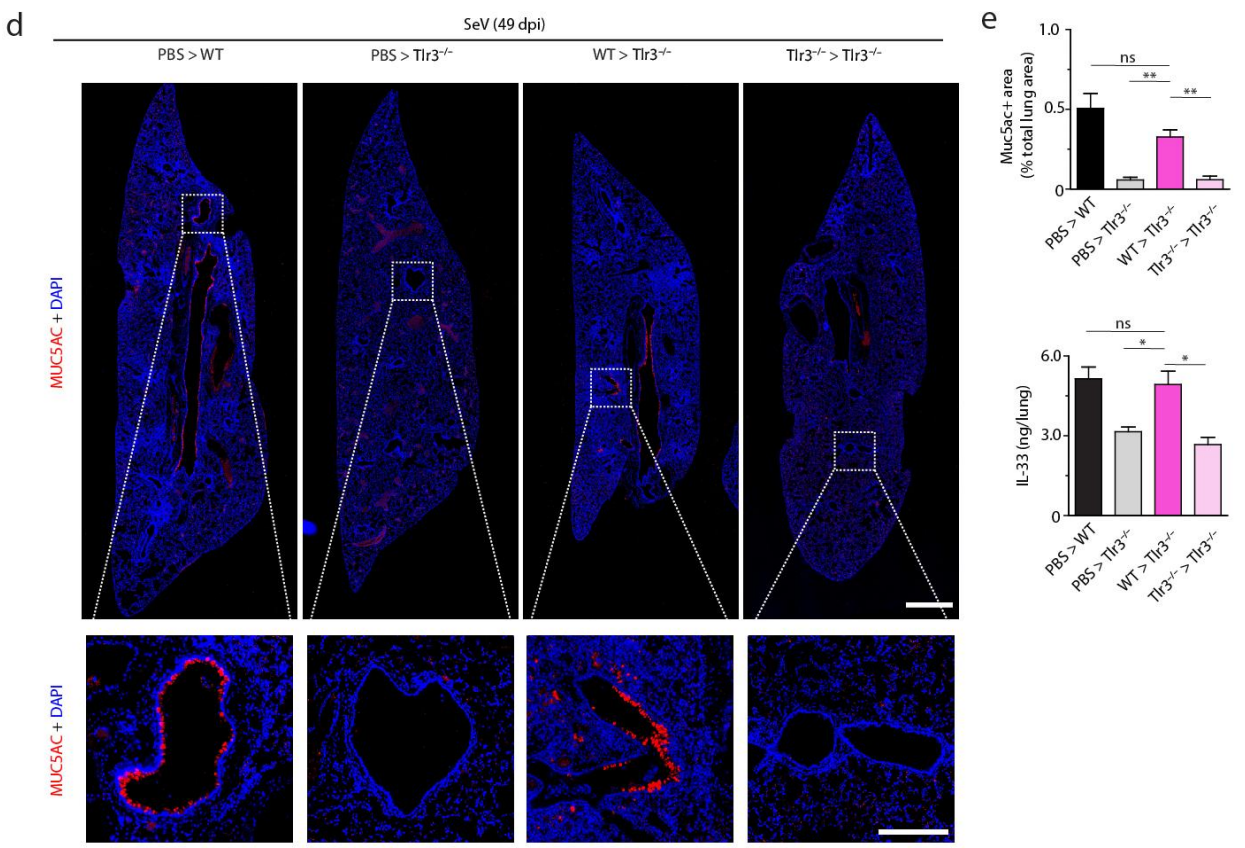

Fig. 6. Adoptive transfer of wildtype moDCs restores chronic disease in *Tlr3*$^{-/-}$ mice. (**a**) Schematic of moDC adoptive transfer from donor mice to recipient mice. (**b**) PAS-hematoxylin staining of lung sections at 49d after SeV infection from *Tlr3*$^{-/-}$ mice that were transferred with either WT or *Tlr3*$^{-/-}$ moDCs prior to SeV infection. Control WT and Tlr3$^{-/-}$ mice were transferred with PBS. (**c**) Quantification of PAS staining and colorized hematoxylin staining. (**d**)*Muc5ac* immunostaining of WT and *Tlr3*$^{-/-}$ mice at 49 d after SeV infection. (**e**) Quantification of *Muc5ac* immunostaining. For (b, d) Scale bars = 500 μm (low mag) and 250 μm (high mag) For (c, e), values are mean ± SEM for 5 mice.

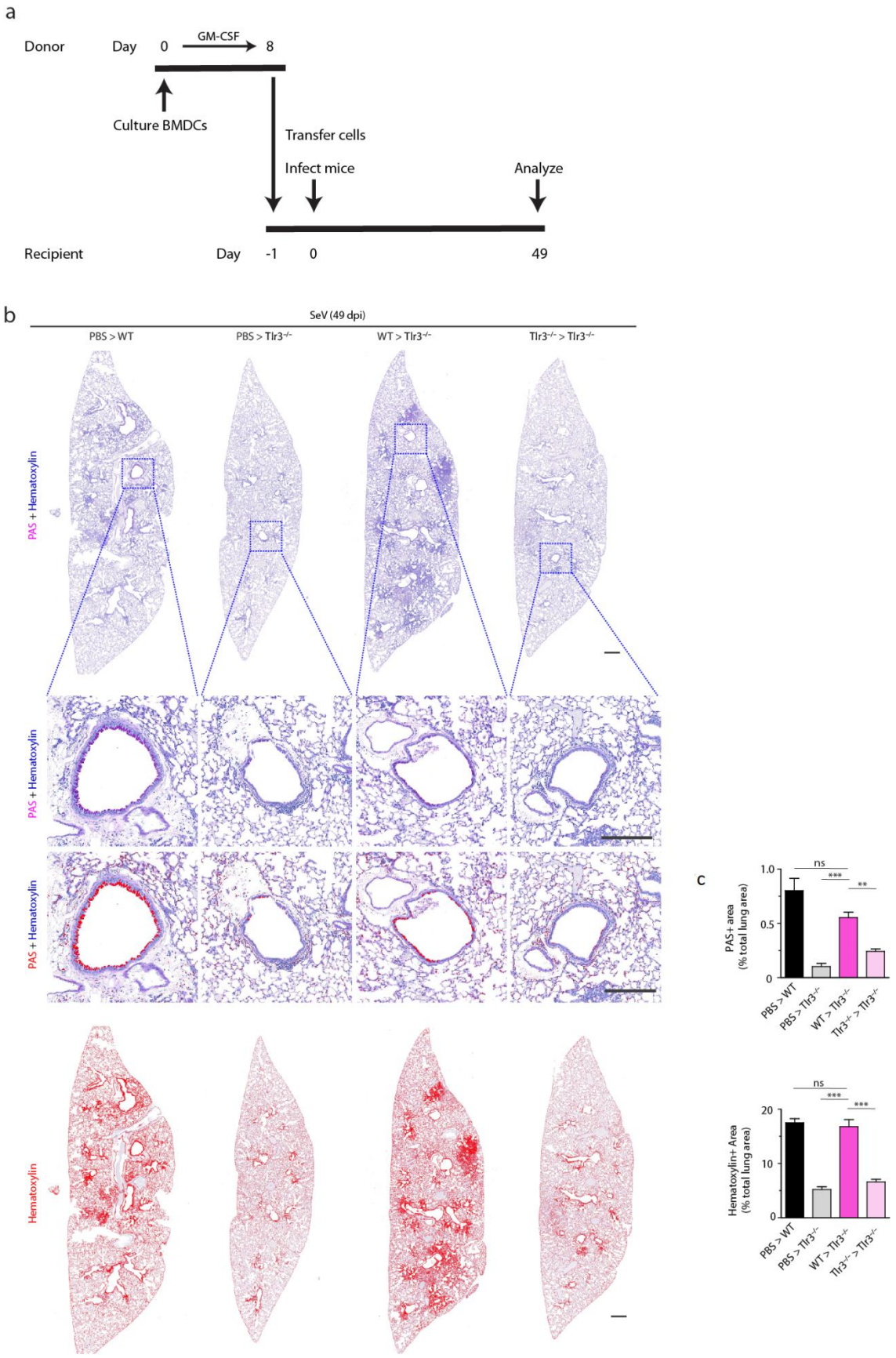
a
Donor
Day 0
GM-CSF
8
Culture BMDCs
Transfer cells
Infect mice
Analyze
Recipient
Day -1 0 49
b
SeV (49 dpi)
PBS > WT
PBS > Tlr3-/-
WT > Tlr3-/-
Tlr3-/- > Tlr3-/-
PAS + Hematoxylin
PAS + Hematoxylin
PAS + Hematoxylin
Hematoxylin
c
PAS+ area (% total lung area)
ns
***
**
1.0
0.5
0
PBS > WT
PBS > Tlr3-/-
WT > Tlr3-/-
Tlr3-/- > Tlr3-/-
Hematoxylin+ Area (% total lung area)
ns
***
***
20
10
0
PBS > WT
PBS > Tlr3-/-
WT > Tlr3-/-
Tlr3-/- > Tlr3-/-

Fig. 7. Adoptive transfer of wildtype BMDCs restores chronic disease in *Tlr3*$^{-/-}$ mice. (**a**) Schematic of BMDC adoptive transfer from donor mice to recipient mice. (**b**) PAS-hematoxylin staining of lung sections at 49d after SeV infection from *Tlr3*$^{-/-}$ mice that were transferred with either WT or *Tlr3*$^{-/-}$ BMDCs prior to SeV infection. Control WT and *Tlr3*$^{-/-}$ mice were transferred with PBS. Scale bars = 500 μm (low mag) and 250 μm (high mag) (**c**) Quantification of PAS staining and colorized hematoxylin staining. Values are mean ± SEM for 5 mice.

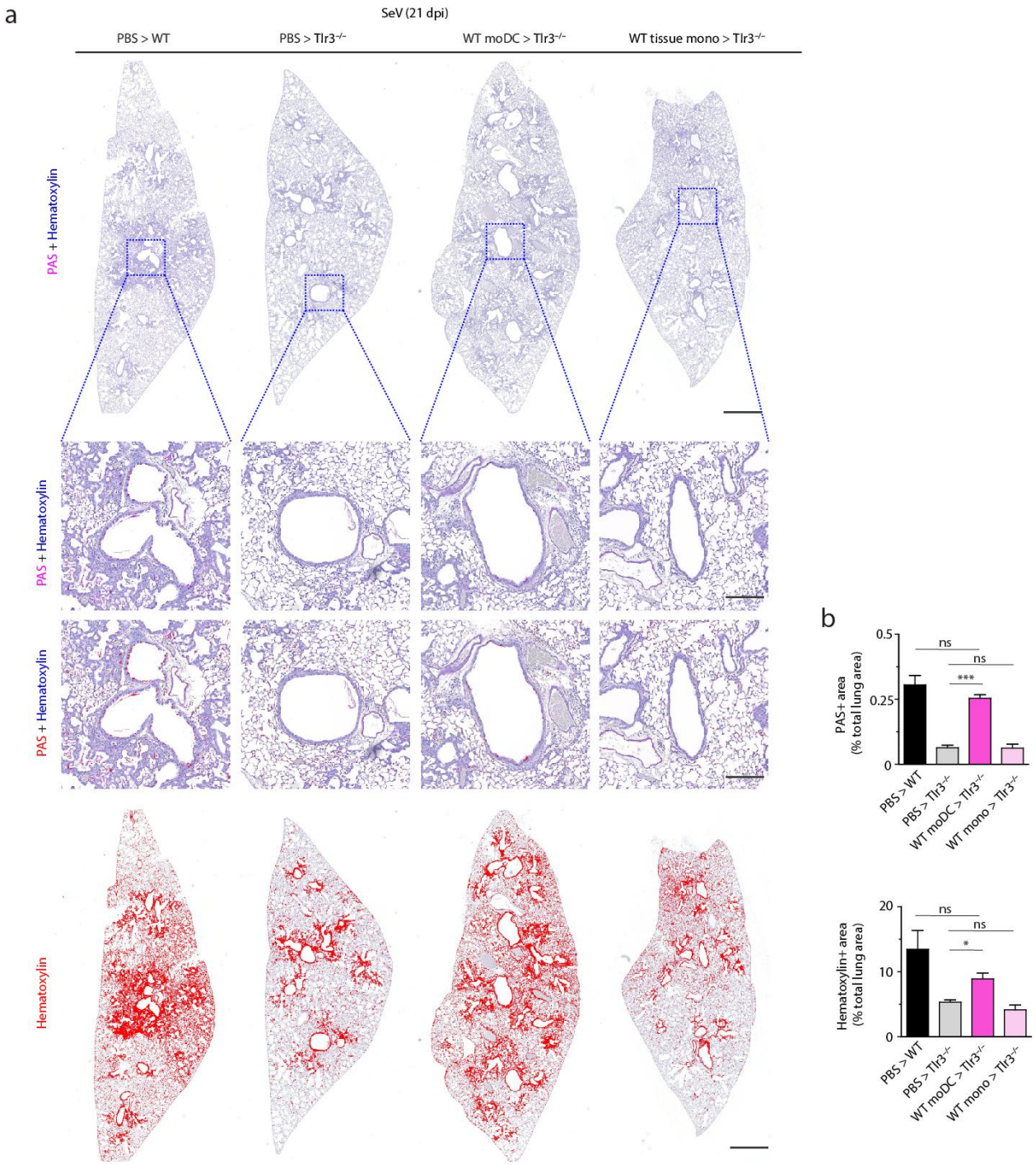

Fig. 8. Adoptive transfer of tissue monocytes does not reconstitute chronic disease. (**a**) PAS-hematoxylin staining of lung sections at 49d after SeV infection from *Tlr3*$^{-/-}$ mice that were

transferred with either WT moDCs or tissue monocytes prior to SeV infection. Control WT and *Tlr3*$^{-/-}$ mice were transferred with PBS. Scale bars = 500 μm (low mag) and 250 μm (high mag) (**b**) Quantification of PAS staining and colorized hematoxylin staining. Values are mean ± SEM for 5 mice.

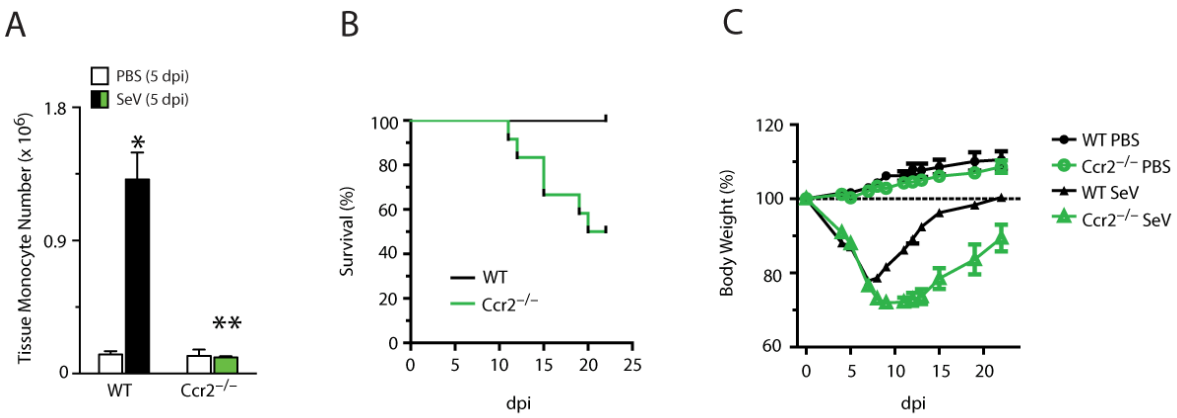

Fig. 9. Effect of Ccr2 blockade on acute disease and DC recruitment (**a**) Whole lung monocyte numbers from *Ccr2*$^{-/-}$ mice at 5 dpi. (**b**) Survival curves and (**c**) body weight timecourse of *Ccr2*$^{-/-}$ animals after SeV infection.

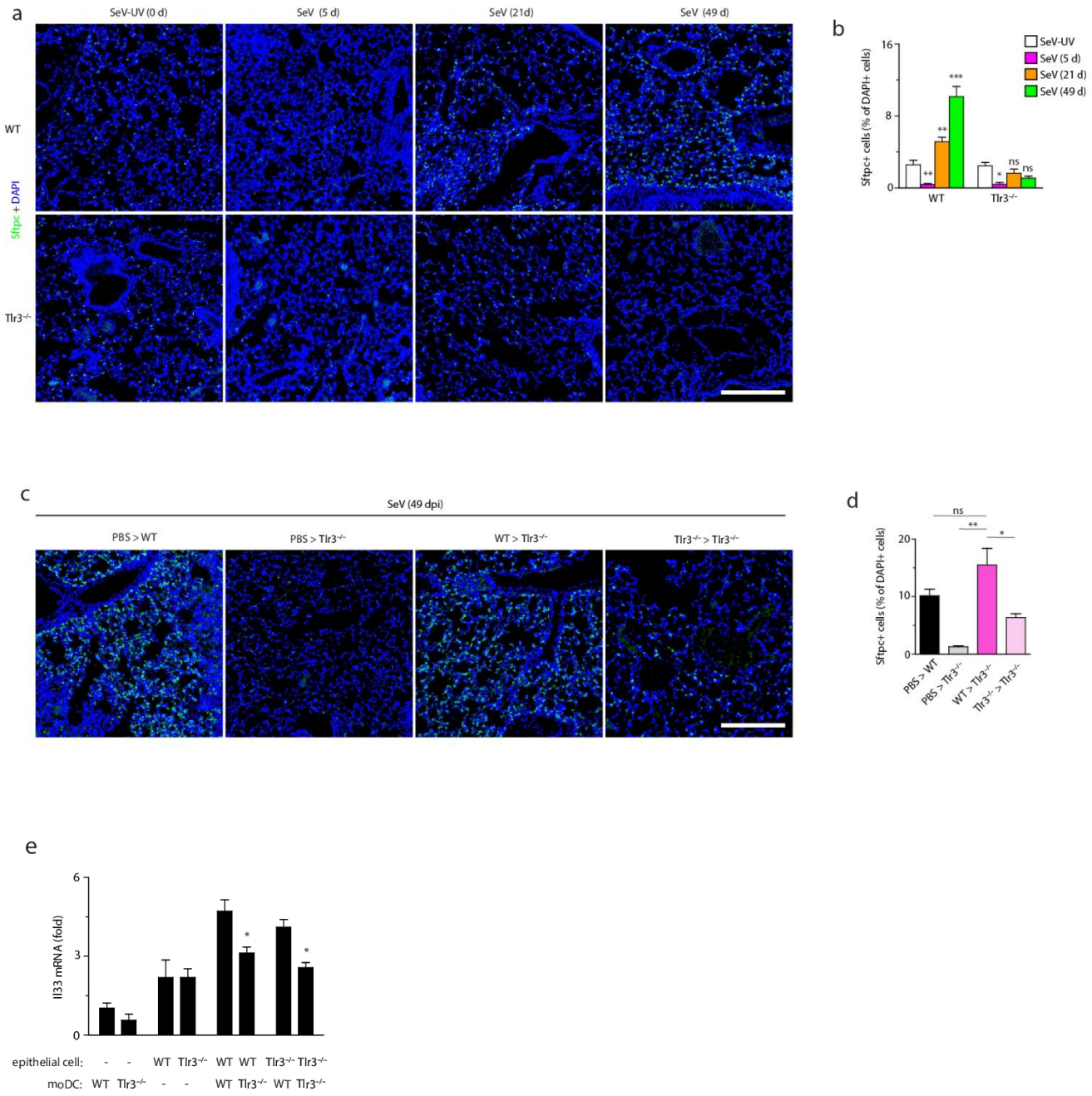

Fig. 10. Tlr3 expression on moDCs is required for AT2 cell proliferation after viral injury. (**a**) Sftpc immunostaining of WT and *Tlr3*$^{-/-}$ lung sections at indicated time points. (**b**) Quantification of Sftpc+ cells as percentage of all DAPI+ cells. (**c**) Sftpc immunostaining of lung sections at 49 dpi from *Tlr3*$^{-/-}$ mice that were adoptively transferred with WT or *Tlr3*$^{-/-}$ moDCs. (**d**) Quantification of

Sftpc+ cells from (c). (**e**) Il33 mRNA levels from co-culture of WT or *Tlr3*$^{-/-}$ naïve epithelial cells with moDCs from WT or *Tlr3*$^{-/-}$ mice sorted at 12 dpi. For (a-c) scale bars = 250 μm.

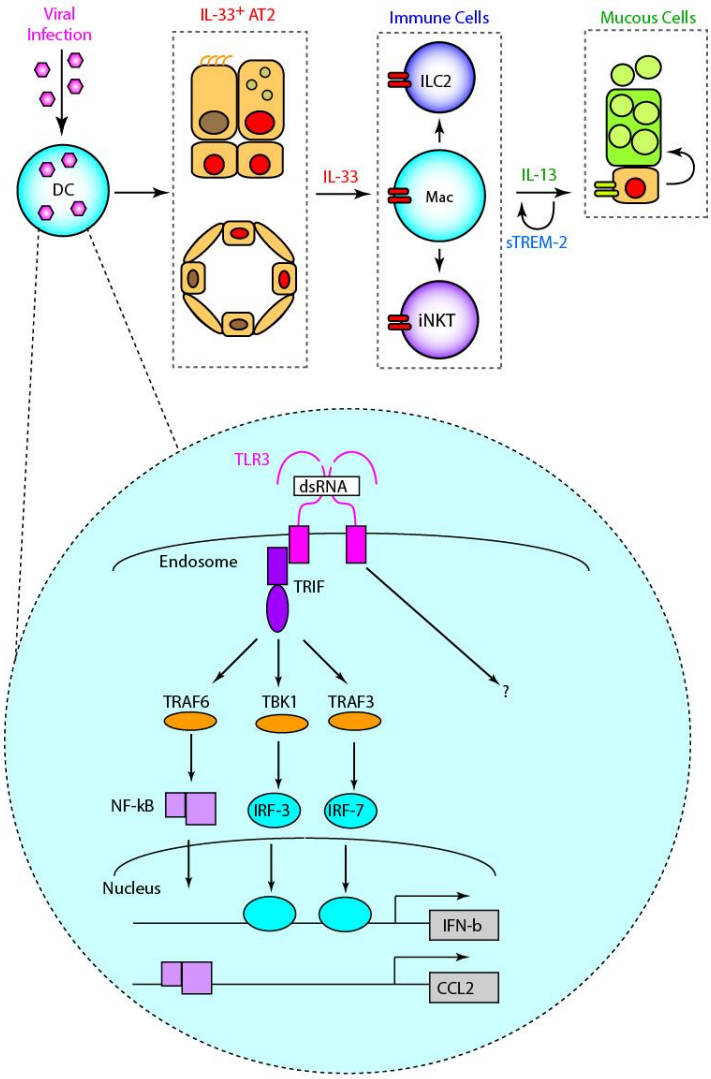

Fig. 11. Schematic for Tlr3 in the development of chronic lung disease. Viral RNA activates Tlr3 signaling in DCs. Trif-mediated signaling leads to subsequent chemokine-dependent recruitment of monocytes into the lung. In addition, an unknown non-canonical TLR3 signaling pathway drives expansion AT2 cells and may also directly induce Il33 expression in AT2 cells. Il33 that is released activates downstream immune cells (ILC2, tissue monocytes, and iNKT cells) to drive Il13 production. In turn, Il13 polarizes macrophages towards type 2 (amplified by sTREM-2) and mucus production in airway epithelial cells that is characteristic of chronic airway disease

Methods

Mouse generation and inoculation

We purchased 6- to 8-week-old wild-type C57BL/6J mice from Jackson Laboratory. We obtained *Tlr3*$^{-/-}$, *Tlr9*$^{-/-}$, and *MDA5*$^{-/-}$ mice from M. Colonna (Washington University, St. Louis, MO), *Tlr7*$^{-/-}$ mice from R. Flavell (Yale University, New Haven, CT), and *Cx3cr1*$^{EGFP/+}$*Ccr2*$^{RFP/+}$ from M. Miller (Washington University, St. Louis, MO). All mouse strains were fully backcrossed onto the C57BL/6 genetic background. We used SeV (Sendai/52, Fushimi strain) to inoculate mice intranasally with virus (1 x 10^5 pfu per mouse) or an equivalent amount of ultraviolet light (UV)-inactivated virus or PBS as described previously (Walter et al., 2001). The Animal Studies Committee of the University approved all experimental protocols.

RNA analysis

We purified RNA from homogenized lung tissue using Trizol Reagent (Invitrogen) or from isolated cells with the RNeasy mini kit (Qiagen), and generated cDNA with the High-Capacity cDNA Archive kit (Applied Biosystems). We quantified target mRNA and viral RNA levels using real-time PCR assay with specific fluorogenic probe-primer combinations and Fast Universal PCR Master Mix systems (Applied Biosystems). Samples were assayed on the 7500 Fast Real-Time PCR System (Applied Biosystems). Levels of specific gene expression were normalized to *Gapdh* mRNA levels.

RNA was then subjected to gene expression analysis using Illumina Mouse-6 V2 BeadChip (Illumina). In brief, mRNA isolated from purified cells was amplified and biotinylated using the Ambion Illumina TotalPrep Kit. Hybridization and scanning, including background correction, was performed according to the manufacturer's instructions using BeadStudio 3.0 software (Illumina).

Microarray normalization and statistical analysis was performed using packages from the Bioconductor project executed in the R programming environment [Gentlemen]. Data were transformed using a variance stabilizing transform [Lin], followed by normalization using robust spline normalization as implemented in the lumi package [Du].

Cell isolation and staining

Lung cell suspensions were prepared from lung tissue subjected to digestion buffer (containing collagenase, hyaluronidase, and DNAse I) for 45 min at 37°C before treatment with ACK buffer to remove red blood cells. The isolated cells were purified using FACS with a MoFlo high-speed flow cytometer (Dako Cytomation) and after FcR blockade, were analyzed for expression of surface markers using a FACSCalibur (BD Biosciences) and FACS-based isolation of cells was performed using Moflo (DAKO-Cytomation) and iCyt Synergy (Sony) . We used the following anti-mouse antibodies: anti-CD11b (eBioscience), anti-Ly6G (BD), anti-Ly6G (BD), anti-F4/80 (eBioscience), anti-CD11c (BD), anti-SiglecF (BD), anti-CD45 (BD), anti-CD64 (BD), anti-CD326 (BD), anti-CD31 (BD). Specific combinations of mAbs were chosen to identify lung tissue monocytes (SSC^{low}, $Ly6G^{-}$, $F4/80^{+}$, $CD11b^{+}$), interstitial macrophages (SSC^{high}, $CD11c^{-}$, $Ly6G^{-}$, $SiglecF^{-}$, $F4/80^{+}$, $CD11b^{+}$), alveolar macrophages (SSC^{high}, $CD11c^{+}$, Ly6G-, $SiglecF^{+}$, $F4/80^{+}$, $CD11b^{-}$), neutrophils (SSC^{high}, $CD11c^{-}$, $F4/80^{-}$, $CD11b^{+}$, $Ly6G^{+}$), eosinophils (SSC^{high}, $CD11c^{-}$, $Ly6G^{-}$, $SiglecF^{+}$, $F4/80^{+}$, $CD11b^{+}$), epithelial cells ($CD45^{-}$, $CD31^{-}$, $CD326^{-}$), endothelial cells ($CD45^{-}$, $CD31^{+}$, $CD326^{-}$) and NKT cells ($TCR\beta^{+}$ CD1d-α-GalCer tetramers). We obtained the APC-labeled α-GalCer-analog (PBS57)-loaded CD1d tetramer from the NIH Tetramer Facility. Dendritic cell subsets were identified as the following: $CD103^{+}$ DCs ($Ly6G^{-}$, $CD11c^{+}$, $SiglecF^{-}$, $CD64^{-}$, $CD103^{+}$, $CD11b^{-}$), $CD11b^{+}$ DCs ($Ly6G^{-}$, $CD11c^{+}$, $SiglecF^{-}$, $CD64^{-}$, $CD11b^{+}$), and monocyte-derived DCs ($Ly6G^{-}$,

CD11c^{+}, SiglecF^{-}, CD64^{+}, CD11b^{+}). Cells were counted using FACS and fluorescent counting beads (CountBright; Life Technologies)

Immunohistochemistry.

Lung tissue was fixed with 10% formalin, embedded in paraffin, cut into 5 μm sections and placed on charged slides. Prior to staining, sections were deparaffinized in Fisherbrand® CitroSolv® (Fisher), hydrated, and heat-treated with antigen unmasking solution (Vector Laboratories, Inc). The following primary antibodies were used for immunostaining: anti-Muc5ac (Fisher; clone 45M1), anti-mouse IL-13 (R&D Systems), anti-Sftpc (Abcam). Sections were incubated in AlexaFluor 488 or 594-conjugated secondary antibodies and counterstained with DAPI-containing mounting media (Vector Labs), before quantification using ImageJ software from the NIH as described previously (Kim et al., 2008).

ELISA

Lung tissues were homogenized in T-PER™ Tissue Protein Extraction Reagent (Fisher) with protease inhibitor cocktail (cOmplete; Roche) and Halt™ phosphatase inhibitor cocktail (Fisher) using a rotor homogenizer (Tissue-Tearor; Biospec Products). Levels of IL-33, Ccl2 and Ccl7 were measured using Duoset ELISA kits (R&D systems) and Instant ELISA kits (eBioscience), respectively and normalized to total lung protein.

Adoptive transfer

Bone marrow derived dendritic cells (BMDCs) were cultured in RPMI in 10% FBS and 20 ng/mL recombinant mouse GM-CSF (Peprotech) for 8 d at 37 °C. Half of the media was changed on day 3 and day 6. For adoptive transfer, cultured BMDCs or moDCs that were FACS-purified from mice at

12 d after SeV infection were delivered intranasally (1 x 10^6 cells in 30 μl of PBS) to recipient mice as described previously (Grayson et al., 2007; van Rijt et al., 2005). Control recipient mice were treated with PBS alone. Mice were infected with SeV 24 hrs after adoptive transfer.

Synthesis and ^{64}Cu radiolabeling of DOTA-ECL1i.

ECL1i (DLeu-Gly-DThr-DPhe-DLeu-DLys-DCys) (1.562 mg, 0.2 μmol) and maleimido-mono-amide-DOTA (1.573 mg, 0.2 μmol) (Macrocyclics) conjugation was performed in pH 7.4 phosphate buffer at 4ºC overnight. The crude conjugate was purified by HPLC to reach 99% chemical purity and characterized by mass spectrometry, which confirmed the presence of one DOTA per peptide (M^+ calculated 1306.65, found: 1306.69, ABI 4700 MALDI TOF-TOF). DOTA-ECL1i (10 μg, 7.66 nmol) was incubated with ^{64}Cu (2 mCi) in 50 μL of 0.1 M pH 5.5 NH_4OAc buffer at 43 ºC for 1 hour, with a yield of 95.6% ± 2.8% (n=12). The specificity activity of ^{64}Cu-DOTA-ECl1i was determined as 261 ± 7.6 μCi/nmol.

Co-culture

We purified lung epithelial cells and lung moDCs using FACS (BD FACSAria IIu). We then incubated the cells together in 96 round bottom wells (5 ×10^4 epithelial cells/well and 2.5 * 10^5 moDCs/well) for 48 hrs at 37C in MTEC/Plus media without EGF (DMEM:F-12, 15 mM HEPES, 3.6 mM sodium bicarbonate, 4 mM L-glutamine, 100 u/ml penicillin/streptomycin, 0.25 ug/ml fungizone, 10 ug/ml insulin, 5 ug/ml transferrin, 0.1 ug/ml cholera toxin, 30 ug/ml bovine pituitary extract, 10% FBS. We isolated cellular RNA for real-time PCR assay of Il33 mRNA and collected cell supernatants for the corresponding protein concentrations of cytokines using ELISA (R&D Systems).

CCR2 blockade

We treated animals with MC-21 antibody (gift from Dr. Matthias Mack) or IgG2b isotype control antibody (ThermoFisher) intraperitoneal for 5 days (10 μg/mouse/day).

Statistical analysis

All data are presented as mean ± SEM and are representative of at least three independent experiments. Unpaired student's t test and one and two way analysis of variance were used to assess statistical significance between means. Significance threshold was set at $p<0.05$.

References

Agapov, E., J.T. Battaile, R. Tidwell, R. Hachem, G.A. Patterson, R.A. Pierce, J.J. Atkinson, and M.J. Holtzman. 2009. Macrophage chitinase 1 stratifies chronic obstructive lung disease. *Am. J. Respir. Cell Mol. Biol.* 41:379-384.

Byers, D.E., and M.J. Holtzman. 2010. Alternatively activated macrophages as cause or effect in asthma. *Am. J. Respir. Cell Mol. Biol.* 43:1-4.

Chupp, G.L., C.G. Lee, N. Jarjour, Y.M. Shim, C.T. Holm, S. He, J.D. Dziura, J. Reed, A.J. Coyle, P. Kiener, M. Cullen, M. Grandsaigne, M.C. Dombret, M. Aubier, M. Pretolani, and J.A. Elias. 2007. A chitinase-like protein in the lung and circulation of patients with severe asthma. *N. Engl. J. Med.* 357:2016-2027.

Faunce, D.E., K. Sonoda, and J. Stein-Streilin. 2001. MIP-2 recruits NKT cells to the spleen during tolerance induction. *J. Immunol.* 166:313-321.

Gowen, B.B., J.D. Hoopes, M.H. Wong, K.H. Jung, K.C. Isakson, L. Alexopoulou, R.A. Flavell, and R.W. Sidwell. 2006. TLR3 deletion limits mortality and disease severity due to Phlebovirus infection. *J. Immunol.* 177:6301-6307.

Grayson, M.H., D. Cheung, M.M. Rohlfing, R. Kitchens, D.E. Spiegel, J. Tucker, J.T. Battaile, Y. Alevy, L. Yan, E. Agapov, E.Y. Kim, and M.J. Holtzman. 2007. Induction of high-affinity IgE receptor on lung dendritic cells during viral infection leads to mucous cell metaplasia. *J. Exp. Med.* 204:2759-2769.

Grayson, M.H., R. Kitchens, E. Agapov, and M.J. Holtzman. 2008. IFNAR signaling to neutrophils is necessary to induce high-affinity receptor for IgE (FcεRI) and activate the conventional dendritic cell (cDC) to T helper type 2 (Th2) cell immune axis after viral infection. *Am. J. Respir. Crit. Care Med.* 177:A84.

Holtzman, M.J. 2012. Asthma as a chronic disease of the innate and adaptive immune systems responding to viruses and allergens. *J. Clin. Invest.* 122:2741-2748.

Holtzman, M.J., D.E. Byers, J. Alexander-Brett, and X. Wang. 2014. The role of airway epithelial cells and innate immunce cells in chronic respiratory disease. *Nat Rev Immunol* 14:686-698.

Hutchens, M., M.E. Luker, P. Sottile, J. Sonstein, N.W. Lukacs, G. Nune, J.L. Curtis, and G.D. Luker. 2008. TLR3 increases disease morbidity and mortality from vaccinia infection. *J. Immunol.* 180:483-491.

Kim, C.H., E.C. Butcher, and B. Johnston. 2002. Distinct subsets of human Va24-invariant NKT cells: cytokine responses and chemokine receptor expression. *Trends Immunol.* 23:516-519.

Kim, E.Y., J.T. Battaile, A.C. Patel, Y. You, E. Agapov, M.H. Grayson, L.A. Benoit, D.E. Byers, Y. Alevy, J. Tucker, S. Swanson, R. Tidwell, J.W. Tyner, J.D. Morton, M. Castro, D. Polineni, G.A. Patterson, R.A. Schwendener, J.D. Allard, G. Peltz, and M.J. Holtzman. 2008. Persistent activation of an innate immune response translates respiratory viral infection into chronic inflammatory lung disease. *Nat. Med.* 14:633-640.

Le Goffic, R., V. Balloy, M. Lagranderie, L. Alexopoulou, N. Escriou, R.A. Flavell, M. Chignard, and M. Si-Tahar. 2006. Detrimental contribution of the Toll-like receptor (TLR)3 to influenza A virus-induced acute pneumonia. *PLoS Pathog.* 2:e53.

Lopez, C.B., B. Moltedo, L. Alexopoulou, L. Bonifaz, R.A. Flavell, and T.M. Moran. 2004. TLR-independent induction of dendritic cell maturation and adaptive immunity by negative-strand RNA viruses. *J. Immunol.* 173:6882-6889.

Lukacs, N.W., J.J. Smit, S. Mukherjee, S.B. Morris, G. Nunez, and D.M. Lindell. 2010. Respiratory virus-induced TLR7 activation controls IL-17 associated increased mucus via IL-23 regulation. *J. Immunol.* 185:2231-2239.

Molet, S., C. Belleguic, H. Lena, N. Germain, C.P. Bertrand, S.D. Shapiro, J.M. Planquois, P. Delaval, and V. Lagente. 2005. Increase in macrophage elastase (MMP-12) in lungs from patients with chronic obstructive pulmonary disease. *Inflamm. Res.* 54:31-36.

Okano, S., Y. Yonemitsu, K. Shirabe, Y. Kakeji, Y. Maehara, M. Harada, Y. Yoshikai, M. Inoue, Hasegawa, and K. Sueishi. 2011. Provision of continuous maturation signaling to dendritic cells by RIG-I-stimulting cytosolic RNA synthesis of Sendai virus. *J. Immunol.* 186:1828-1839.

Shaheen, S. O., D. Barker, and S.T. Holgate. 1995. Do Lower Respiratory Tract Infections in Early Childhood Cause Chronic Obstructive Pulmonary Disease? American Journal of Respiratory and Critical Care Medicine 151:1649-1652

Pulendran, B., H. Tang, and S. Manicassamy. 2010. Programming dendritic cells to induce T(H)2 and tolerogenic responses. *Nat Immunol* 11:647-655.

Rudd, B.D., J.J. Smit, R.A. Flavell, L. Alexopoulou, M.A. Schaller, A. Gruber, A.A. Berlin, and N.W. Lukacs. 2006. Deletion of TLR3 alters the pulmonary immune environment and mucus production during respiratory syncytial virus infection. *J. Immunol.* 176:1937-1942.

Savage, A.K., M.G. Constantinides, J. Han, D. Picard, E. Martin, B. Li, O. Lantz, and A. Bendelac. 2008. The transcription factor PLZF directs the effector program of the NKT cell lineage. *Immunity* 29:391-403.

Shornick, L.P., A.G. Wells, Y. Zhang, A.C. Patel, G. Huang, K. Takami, M. Sosa, N.A. Shukla, E. Agapov, and M.J. Holtzman. 2008. Airway epithelial versus immune cell Stat1 function for innate defense against respiratory viral infection. *J. Immunol.* 180:3319-3328.

Takeuchi, O., and S. Akira. 2010. Pattern recognition receptors and inflammation. *Cell* 140:805-820.

Tupin, E., and M. Kronenberg. 2006. Activation of natural killer T cells by glycolipids. *Methods Enzymol.* 417:185-201.

Tyner, J.W., E.Y. Kim, K. Ide, M.R. Pelletier, W.T. Roswit, J.D. Morton, J.T. Battaile, A.C. Patel, G.A. Patterson, M. Castro, M.S. Spoor, Y. You, S.L. Brody, and M.J. Holtzman. 2006. Blocking airway mucous cell metaplasia by inhibiting EGFR antiapoptosis and IL-13 transdifferentiation signals. *J. Clin. Invest.* 116:309-321.

Tyner, J.W., O. Uchida, N. Kajiwara, E.Y. Kim, A.C. Patel, M.P. O'Sullivan, M.J. Walter, R.A. Schwendener, D.N. Cook, T.M. Danoff, and M.J. Holtzman. 2005. CCL5-CCR5 interaction provides antiapoptotic signals for macrophage survival during viral infection. *Nat. Med.* 11:1180-1187.

van Rijt, L.S., S. Jung, A. Kleinjan, N. Vos, M. Willart, C. Duez, H.C. Hoogsteden, and B.N. Lambrecht. 2005. In vivo depletion of lung CD11c+ dendritic cells during allergen challenge abrogates the characteristic features of asthma. *J. Exp. Med.* 201:981-991.

Walter, M.J., N. Kajiwara, P. Karanja, M. Castro, and M.J. Holtzman. 2001. IL-12 p40 production by barrier epithelial cells during airway inflammation. *J. Exp. Med.* 193:339-352.

Wang, Q., D.J. Miller, E.R. Bowman, D.R. Nagarkar, D. Schneider, Y. Zhao, M.J. Linn, A.M. Goldsmith, J.K. Bentley, U.S. Sajjan, and M.B. Hershenson. 2011. MDA5 and TLR3 initiate pro-inflammatory signaling pathways leading to rhinovirus-induced airways inflammation and hyperresponsiveness. *PLoS Pathog.* 7:e1002070.

Wang, T., T. Town, L. Alexopoulou, J.F. Anderson, E. Fikrig, and R.A. Flavell. 2004. Toll-like receptor 3 mediates West Nile virus entry into the brain causing lethal encephalitis. *Nat. Med.* 10:1366-1373.

Wu, K., D.E. Byers, X. Jin, E. Agapov, J. Alexander-Brett, A.C. Patel, M. Cella, S. Gilfilan, M. Colonna, D.L. Kober, T.J. Brett, and M.J. Holtzman. 2015. TREM-2 promotes M2 macrophage survival and airway disease after respiratory viral infection. *J. Exp. Med.* 212:681-697